



## Research paper

## First-principles algorithms for ship motion simulation based on ARMA and trochoidal wave models

Alexander Degtyarev<sup>a,\*</sup>, Vasily Khramushin<sup>a,b</sup><sup>a</sup> St.Petersburg State University, Russia<sup>b</sup> Krylov Engineering Society, Russia

## A B S T R A C T

An approach for the direct simulation of ship behavior in heavy sea conditions using modern computers methods is described. The approach includes a model for wind-driven waves, algorithms for hydrodynamic pressure calculation, a solution of the diffraction problem, and the integration of the approach into a problem solution environment. An ARMA (autoregressive-moving average) model is used for the simulation of a hydrodynamically adequate spatial-temporal wave surface and integrated with a calculation of hydrodynamic pressure at any point under the wave surface. The integration of the wave pressure over the ship hull and the solution of the diffraction problem provides the excitation forces and moments and permits direct numerical simulation of ship motions in waves. An effective numerical implementation of the algorithms with mapping to modern computer architecture is described. The combination of the numerical algorithms with a visual simulation environment is presented as a virtual testbed.

## 1. Introduction

The behavior of a ship in ocean waves is usually described by a system of second order ordinary differential equations, which are obtained under the assumption that the ship is a rigid body located on the water-air interface in a gravity wave field. In this case, the ship has 6°-of-freedom. It is taken out of the equilibrium position due to wind-driven waves as well as the wind itself. In this case, the balance of forces consists of the ship's inertia forces, the disturbing forces of waves and wind, resistance and propulsion forces, as well as restoring forces in the free degrees of freedom (heave, pitch, roll). With this approach, many traditional ways of representing ship dynamics models are attempts to develop analytical representations of different categories of forces and moments. The restoring component is most often represented by a linear or power-law polynomial according to the components of the degrees of freedom. The damping component is approximated by a linear or power-law velocity term of the corresponding degree of freedom. Expressions for the excitation forces and moments are derived based on the representation of the wave motion of the fluid as a potential flow. In this case, the final expressions in some approximation for hydrodynamic forces and moments can be obtained only in the case of a harmonic wave. Multi-frequency excitations lead to extremely complex expressions, which, moreover, are of little use. The use of the concept of stochastic potential has not yet led to tangible results in the representation of the disturbing forces.

Traditionally, multivariable potential flow decomposition (Newman, 1970; Lugovski, 1980; Voitkunski, 1985) is used to obtain finite expressions for disturbance forces, which is valid for oscillations of a sufficiently small, albeit finite amplitude. The velocity potential of the perturbed fluid motion, the elevation of the free surface, and then the pressure and hydrodynamic forces are decomposed by small parameters. The substitution of such expansions into the nonlinear boundary conditions on the free surface of the fluid and on the wetted surface of the vessel, as well as in the Lagrange integral, reduces the complete nonlinear hydrodynamic problem to a sequence of linear problems under the assumption of convergence of the iterative process. The solution to the problem of linear hydrodynamic motion is fundamentally known (Frank, 1967; Khaskind, 1973), but can only be found numerically for real ship forms. Thus, the velocity potential is found as a sum of harmonic functions, each of which satisfies a linearized boundary condition on the equilibrium free surface of the fluid. The kinematic boundary condition on the ship's hull does not explicitly contain nonlinearities with respect to the terms of the potential decomposition and their derivatives, but rather the nonlinearity is hidden in the kinematic characteristics of the motion, which are proportional to the small parameters by which the expansion takes place. In the general case, they depend on the derivatives of the velocity potential through hydrodynamic forces. Therefore, such a linearization of the problem turns out to be only partial. To complete it, it is necessary to establish a quantitative relationship between the decomposition parameters or pre-set the law

\* Corresponding author.

E-mail address: [a.degtyarev@spbu.ru](mailto:a.degtyarev@spbu.ru) (A. Degtyarev).

for the ship's oscillations. In any case, finding the second and higher approximations is a complex numerical problem, possible only for specific hull-section shapes.

It should be noted that the solution of linear problems is no longer the goal of research in any subject area, including ship hydrodynamics. Only nonlinear problems that describe either extreme states or situations with a qualitative change in the behavior of objects are subjects of interest. Therefore, this article focuses on both the reproduction of physically adequate stochastic nonlinear wave disturbances and the nonlinear behavior of the ship in stormy conditions.

The most complete version of the system of nonlinear equations of ship dynamics can be found in (Lugovski, 1995). However, the development of this way to improve the accuracy of modeling the behavior of a ship at sea has led to the understanding that this approach is a dead end. The complexity of the final expressions grows to such limits that it is no longer possible to draw analytical conclusions, and numerical solution and programming encounter serious obstacles in the way of implementation. In addition, the application of the models obtained for use in conditions of irregular waves is extremely difficult, especially when all degrees of freedom are considered (Lugovski, 1995). This conclusion, considering the increased power of computer technology, led to the development of a new approach, which consists in direct simulation of the behavior of a marine object under the action of external excitations. Such an approach, of course, precludes the possibility of drawing analytical conclusions, building asymptotic solutions, or developing qualitative understandings, but it does make it possible to conduct computational experiments, which, with the current level and development of computer technology, allow us to consider them as the results of a full-scale experiment, or in other words "physics in the form of a model."

This idea is not new. Over the last 50 years, other methods for numerical modeling of ship dynamics in waves have been developed. They represent the use of CFD methods for external forcing and ship dynamics modeling. For this purpose, it is possible to apply a URANS model with closing relations in the form of a turbulence model for the boundary layer, such as Shear Stress Transport (SST) model (Balashov et al., 2018), Spectral Wave Explicit Navier-Stokes Equations (SWENSE) (Gong et al., 2022, etc.). It is possible to directly use any off-the-shelf frameworks and CFD software, for example, such as open-source code Open-FOAM (Yu et al., 2023) to implement hybrid methods for ship dynamics modeling. LAMP solution (Shin et al., 2003) and many other different hybrid and CFD solutions are known. However, all the proposed solutions have high computational cost. The reasons are (1) the high computational complexity of numerically solving the Navier-Stokes Equations in its finite-difference representation; (2) the iterative procedure to reconstruct the wave profile around the ship; (3) the high computational cost in computing the incoming wave profile at grid points on the hull due to the computation of a large number of trigonometric functions (Shin et al., 2003). All of this makes it impossible to use such approach effectively.

The approach proposed in the article is called a virtual testbed (Bogdanov et al., 2020), which can completely replace a full-scale trial (and even more so a model experiment) under conditions for which the physics of the phenomenon under consideration is completely known. In this situation, completely new requirements arise for the nature and type of components of the general simulation model. First, a hydrodynamically adequate and computationally efficient model of ocean waves and wind is required. Secondly, an effective procedure for the direct simulation of the dynamics of the interaction between a vessel and the environment must be built. This model should (1) take into account the space-temporal distribution of hydrodynamic pressures under the free surface generated by the wave model; (2) take into account diffraction and other effects of ship-wave interaction, which leads to a redistribution of pressure over the hull and a change in the magnitude of external forces and moments.

Here it is necessary to note the methodological difference between

the formulation of mathematical models of ship motion in the form of differential equations and direct simulation. In the first case, the components are grouped around derivatives of the same order. In the second case, the decomposition is by forces of different nature. For example, energy dissipation based on the first derivative of a process is composed of radiation type process and friction. Radiation type process have already been taken into account when the forces of potential flow are modeled. At the same time additional components are needed to account for frictional resistance. We have approximately the same reasoning concerning the concept of added masses, which are traditional in the classical approach of using differential equations as mathematical models of ship dynamics.

The efficiency of any computational algorithm depends on the completeness of the processor capabilities utilization and the use of built-in operations. Such possibilities include, for example, the simultaneous execution of several operations of the same type. To use such instructions, it is necessary to present all computational algorithms in a form that allows one to work with data sets (vectors).

This approach is relevant both for vector processors and when using GPGPU or the OpenGL API. It is known that the speed-up of calculations in this case is determined by the degree of vectorization of the numerical algorithm (Ortega, 2013). Therefore, it is important to present a description of the hull, equations and dependencies in tensor form.

The authors have, at different times, developed separate components of this complex task. This article is focused on the presentation of the results of combining these components to achieve the final result, which is organizing the process of direct computational experiments on a modern computer.

In the theoretical and algorithmic part of this work, mathematical tools for the practical construction of direct computational experiments with the possibility of visually illustrative computer tests of the ship's seaworthiness are presented and discussed. This approach is useful both at the stages of engineering surveys for designing the optimal lines and general naval architecture of ships and vessels of improved seaworthiness, and in testing the modes of efficient and safe deployment of ships and vessels of the operating fleet.

In the developed software, which is called "Vessel," different ocean wave models are used, which allows the solution of specific computational experiments.

In a complete computational experiment with an arbitrary ship speed and course, three models of dynamics are implemented: 1) hydrostatic balancing of the submerged hull on the waves; 2) undistorted wave field with velocity head and compensating vortex sources near the vessel's hull surface; 3) complete hydrodynamic modeling of wave formation and wave flow near the vessel, with diffraction of waves by the ship's hull.

## 2. Wave simulation ARMA model

Real ocean waves are characterized by their irregular character and three-dimensional structure. Currently, the most popular models for describing wind waves are models based on the linear expansion of a stochastic moving surface as a system of independent random variables. The most popular model is that of Longuet-Higgins (1962), which is based on a stochastic approximation of the moving wave-front as a superposition of elementary harmonic waves with random phases and random amplitudes,  $c_n$ ,  $\epsilon_n$ :

$$\zeta(x, y, t) = \sum_n c_n \cos(u_n x + v_n y - \omega_n t + \epsilon_n) \quad (1)$$

where the wave number  $(u_n, v_n)$  is continuously distributed on the  $(u, v)$  plane, i.e. the unit area  $du \times dv$  contains an infinite number of wave numbers. The frequency  $\omega_n$  associated with wave numbers  $(u_n, v_n)$  is given by the dispersion relation

$$\omega_n = \omega(u_n, v_n) \quad (2)$$

The phase  $\epsilon_n$  are jointly independent random variables uniformly distributed in the interval  $[0, 2\pi]$ .

The popularity of this kind of models is due to their hydrodynamic nature. The linear solution of the Laplace equation describing the behavior of wind waves looks like this, so we can say that such a representation has a physical sense. However, that is the very reason such models have certain limitations, since their physical meaning is associated with the solution of a linear problem. Therefore, the Longuet-Higgins (1962) model and other models close to it (St. Denis and Pierson, 1953; Rosenblatt, 1957; Sveshnikov, 1959) represent smooth waves of small amplitude well. Indeed, the Longuet-Higgins model is the sum of random variables at each time point. The more terms, the closer the result to the normal distribution law, regardless of what distribution each random component  $c_n$  and  $\epsilon_n$  has. It is known that the normal distribution law of a random process corresponds to the linear case. At the same time, for a long realization of a random process, a sufficiently large set of components of elementary harmonics is required, since the repetition period of the implementation is equal to the lowest common multiple of the periods of these elementary waves.

Thus, these popular models cannot be used to simulate very long realizations, as well as asymmetric storm waves, trochoidal waves, etc.

Another approach to modelling wind waves is possible representing the sea surface as a stochastic moving surface formed by a linear transformation of white noise with memory. These methods are one of the most popular ways of modelling stationary ergodic Gaussian random processes with given correlation characteristics (Box et al., 2008). However, these methods have not been used to simulate wind waves in recent times. The formal mathematical framework was developed by Gургенидзе and Трапезников (1988) and Rozhkov and Trapeznikov (1990). They built a one-dimensional model of ocean waves  $\zeta(t)$ , on the basis of an autoregressive-moving average (ARMA) model

$$\zeta_t = \sum_{i=1}^N \Phi_i \zeta_{t-i} + \sum_{j=1}^P \Theta_j \epsilon_{t-j} \quad (3)$$

here  $\Phi_j$  are the autoregressive parameters,  $\Theta_j$  are the parameters of the moving average, and  $\epsilon_j$  is white noise with an infinitely divisible distribution law.

More recently, the ARMA approach has been extended to any random scalar field (Degtyarev and Boukhanovsky, 2000; Boukhanovsky et al., 2001, etc.). For example, a discrete model applicable to a moving wavy surface in three dimensions (2-D space + 1-D temporal) can be defined as

$$\zeta_{x,y,t} = \sum_{i=1}^{N_x} \sum_{j=1}^{N_y} \sum_{k=1}^{N_t} \Phi_{i,j,k} \zeta_{x-i,y-j,t-k} + \epsilon_{x,y,t} \quad (4)$$

where  $\Phi_{i,j,k}$  are the generalized coefficients of the AR, and  $\epsilon_{x,y,t}$  is a field of white noise.

The procedure for estimating the parameters of the AR and dispersion of the field of white noise is carried out using the autocovariance function (ACF) using Yule-Walker equations (Box et al., 2008; Gургенидзе and Трапезников, 1988; Rozhkov and Trapeznikov, 1990). An example wave field simulation generated using an AR model is shown in Fig. 1.

This model has turned out to be very effective both in terms of computational efficiency and in reproduction of physical phenomena. In Degtyarev and Gankevich (2011) the computational efficiency of parallel algorithms for generating wind-wave fields are presented. Degtyarev and Reed (2013) and Degtyarev et al., 2019 contain the results of verification of the ARMA model against a vast amount of natural oceanographic data. Verification results show full agreement of full-scale observations with modeling results for the following general one-dimensional characteristic:

- distribution of wave heights

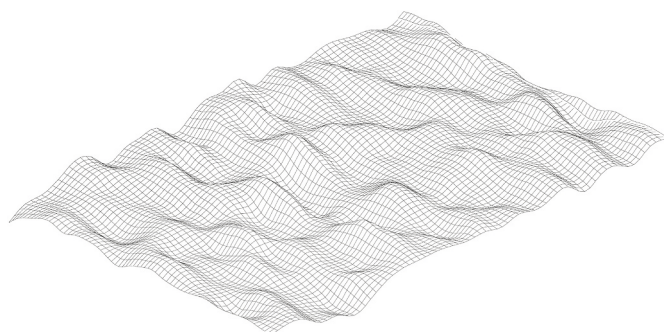


Fig. 1. 3D wave field (AR modeling).

- distribution of wave steepness,
- distribution of wavelengths
- distribution of the lengths of the crests
- distribution of wave periods

In addition, unlike many other known wave models, ARMA makes it possible to capture the multivariate statistical characteristics of the waves. Typical indicators of statistical dependence of random variables are the first and second central moments of their joint distribution—via curves of regression (conditional mean value)

$$m_h(\lambda) = \int_{-\infty}^{\infty} hf(h|\lambda) dh \quad (5)$$

and skedasticity (error with constant variance):

$$\sigma_m^2(\lambda) = \int_{-\infty}^{\infty} (h - m_h(\lambda))^2 f(h|\lambda) dh \quad (6)$$

The ability of ARMA to reproduce both the univariate and multivariate statistical characteristics of waves is logically complemented by the ability to reproduce the dispersion properties of waves.

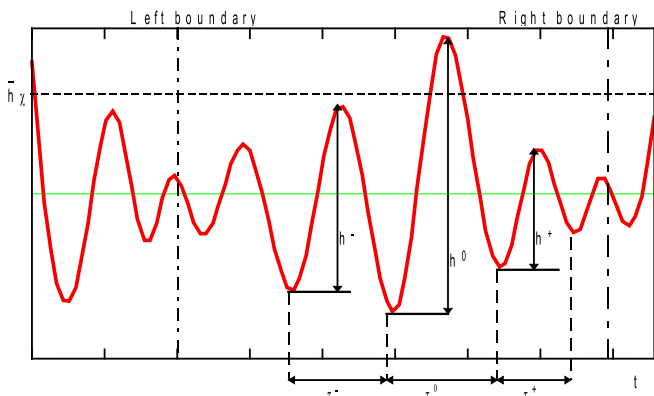
Fig. 18 in Degtyarev and Reed (2013) shows results for wave measurements corresponding to sea states 5 and 8. The measurements were taken at a single-point in the towing tank at Kaliningrad Institute of Technology. An analysis of wave slope spectrum and wave amplitude spectrum for these cases has been carried out. These spectra were used for time domain process generation. This picture shows the results of the reconstruction of the dispersion relation  $k(\omega)$  based on the integration of the equation for the changes with the spatial coordinates  $X$ , for three synchronous wave records.

Based on the results of these three studies, Degtyarev and Reed (2013) conclude that the proposed autoregression model of ocean waves in quasi-stationary conditions has acceptable physical characteristics.

ARMA is also able to model the group structure of wind waves. The group structure of wind waves is a very important phenomenon for modelling ship motions in storms (Boccotti, 2000, 2014), especially for critical wave groups (Anastopoulos et al., 2015). It was verified with the help of the following specific experimental data (Rozhkov and Lyashenko, 1990):

- distribution of the wave numbers in groups;
- correlation of characteristic waves in wave groups;
- distribution of maximum wave height in extreme groups;
- average time between groups and their distribution, etc.

Let us consider the basic statistical characteristics of wave groups. Since in marine applications it is necessary to account for the probabilities of the appearance of several waves with height over some threshold, let us use the concept of group intensity (Rozhkov and Lyashenko, 1990). The group is a set of successive waves where the highest (main) wave exceeds a certain level  $\gamma$ . The level is usually taken as the ratio of the wave height of a given probability to the average wave

Fig. 2. Typical wave group,  $n = 6$ .

height calculated over the entire sample population.

A typical wave group is shown at Fig. 2.

The following wave groups elements are considered: the height of main wave in a group  $h^0$ , the number of waves in a group  $n$ , the relative height of waves in a group to the left and to the right of the main  $h^-/h^0$  and  $h^+/h^0$ , the relative periods of waves to the left and to the right of the main  $\tau^+/\tau^0$ ,  $\tau^-/\tau^0$ , and the time period between two sequential extreme groups  $S$ .

First, the first (and sometimes the second) statistical moments of these values are estimated. The average (over all realizations) dependence of  $m_\chi(h^0/h)$  is presented in Fig. 3. Here the dots indicate the results from experiments.

In addition to the analysis of characteristic moments, the distribution laws of different group elements were compared. In Fig. 4 on the grid of a truncated Rayleigh distribution

$$F(h, \chi) = 1 - \exp \left[ -\frac{\pi}{4} (\chi^2 - h^2) \right] \quad (7)$$

empirical estimates of the distribution of the normalized basic wave height in the group (points) and the straight line, which is the average of the model results, are shown. In this case, the results for all  $\chi$  are presented on the grid, which was made possible by introducing a dimensionless argument:

$$\nu = \chi^2 - \left( h^0 / \bar{h} \right)^2$$

Figs. 5 and 6 show additional characteristics at different levels  $\chi$ .

Fig. 7 shows the averaged histogram of the wave number distribution in the group (dashed line) and the empirical histogram for moderate wind waves (solid line).

Generalized statistical characteristics are given in the table below:

Parameter	Empirical	Model
$\bar{n}$	5	5
$\bar{h}^0 / \bar{h}^+$	0.6	0.62
$\bar{h}^0 / \bar{h}^-$	0.6	0.59
$\bar{\tau}^0 / \bar{\tau}^\pm$	1	1

These results show that despite the lack of a physical basis for the ARMA model, it effectively represents both dispersive wave properties and the complex characteristics of wind wave fields: complex waves, group structure, storm evolution, nontrivial statistical characteristics, wave nonlinearity, etc. At the same time, in contrast to the Longuet-Higgins model (Longuet-Higgins, 1962), an ARMA based model can efficiently reproduce very long realizations of a random process. Its length is limited solely by the return period of the random number generator used in (4) to determine  $\varepsilon$ . This makes it possible to obtain

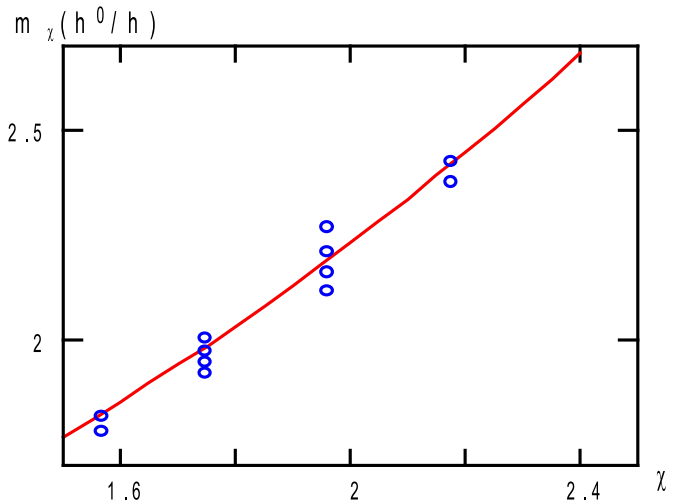


Fig. 3. Average maximum group height.

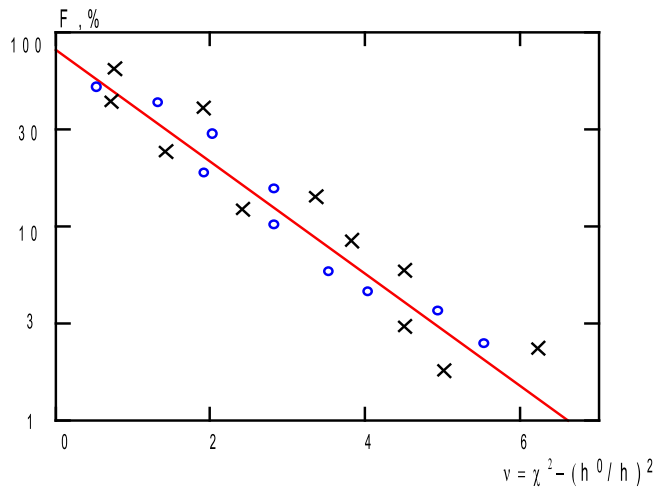


Fig. 4. Distribution of maximum group height (circle – model; cross – combined experimental data; line – truncated Rayleigh distribution law).

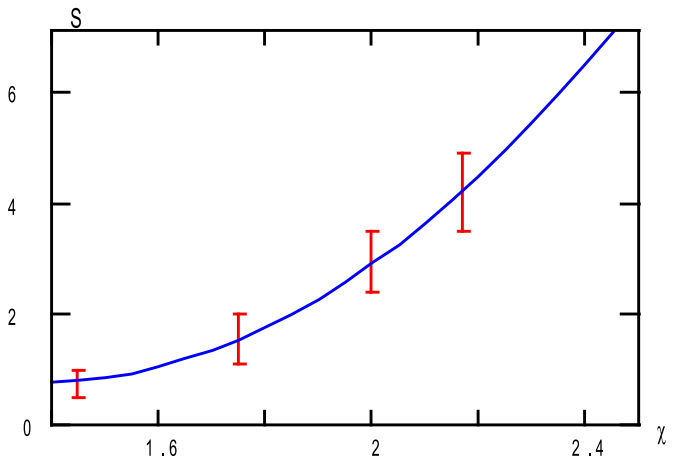


Fig. 5. Average interval between groups with confidence intervals.

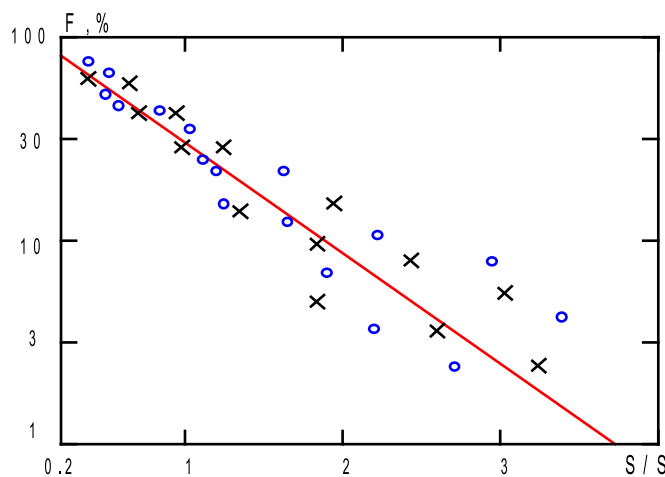


Fig. 6. Distribution of intervals between groups (the same symbols as in Fig. 4).

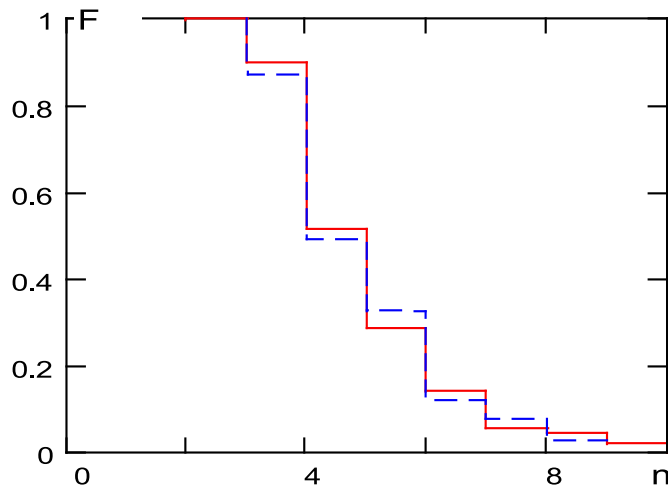


Fig. 7. Distribution of number of waves in groups.

very long realizations of the ship's motion, sufficient to realize the occurrence of rare events.

Modeling of non-linear waves is very important when studying the behavior of a ship in extreme seas (severe storms). In this case, the distribution  $F_\zeta(z)$  of wave elevation  $\zeta(t)$  is non-gaussian. It requires application of nonlinear transformation  $z = f(y)$  to model process  $y(t)$  of ARMA type (5). This transformation corresponds to the solution of a transcendental equation

$$F_\zeta = \Phi(y) \quad (8)$$

where  $\Phi(y)$  is a univariate integral function of a gaussian distribution, or the following expression for mesh function  $\{y_k\}_{k=0}^R$ ,  $\{z_k\}_{k=0}^R$ :

$$F_\zeta(z_k) = \frac{1}{\sqrt{2\pi}} \int_{-\infty}^{y_k} \exp\left[-\frac{t^2}{2}\right] dt \quad (9)$$

However, the correlation function is changed in any nonlinear transformation of stochastic process. To avoid this, a preliminary transformation of the correlation function using Edgeworth's series expansion is used. Thus, it is necessary to compare the model gaussian process with redistributed energy versus frequency to the initial non-gaussian process  $z$ . The redistribution of energy provides a model spectrum  $S_\zeta(\omega)$  that is identical to the initial spectrum  $S_\zeta(\omega)$  after a nonlinear transformation. This procedure is described in detail in

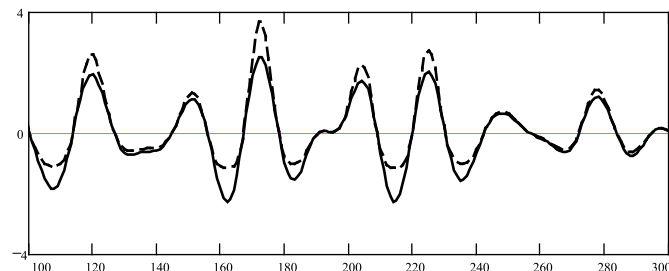


Fig. 8. Realization of Gaussian (solid line) and non-Gaussian (dash line) wave shapes.

(Degtyarev et al., 2014). Realizations of the Gaussian and non-Gaussian waves at a fixed point reproduced with this model are shown in Fig. 8.

The method described above requires knowledge of the distribution function for nonlinear waves and field measurement data. This approach is not always correct, since an arbitrarily defined distribution function is often not physically adequate. In addition, even in the case of nonlinear correction, ARMA cannot reproduce breaking waves, instability and other phenomena associated with the violation of the requirement for wave profile smoothness. In this case (if one does not know the real nonlinear wave distribution function), a simulation can be carried out based on solving the complete hydrodynamic equations. So far, the only example of integrating the hydrodynamic equations for gravity waves in deep water is the Gerstner waves (Gerstner, 1809; Abrashkin and Pelinovsky, 2022). Despite the fact that Krylov (1951) developed the theory of ship motion in waves based on Gerstner's equations, they have not found wide application in mathematical models of ship dynamics. The reason is the difficulty of realizing a Gerstner wave. Unlike other solutions in the field of nonlinear waves (Stokes waves, soliton solutions), the Gerstner wave is vortical and cannot arise in nature under the potential flow assumption (Lagrange's theorem). Approaches to ship dynamics have focused on the construction of mathematical models in the form of differential equations for oscillatory motion in the form of a balance between inertial, damping, restoring and excitation forces/moments due to a surface wave. The last ones were expressed in terms of the velocity potential of the wave motion of the fluid. The specificity of this approach does not allow wide application of the Gerstner solution for practical calculations.

When considering the conditions of a storm, Gerstner waves can be considered to be the best model. It accurately describes the three-dimensional distribution of velocities throughout the water column affecting the ship's hull. However, this is possible only in direct simulation, which will be discussed later in this paper.

It should be noted that a most-independent attempts to implement the ARMA wave mode, partially described in (Weems et al., 2016) were unable to achieve consistent stable solutions for progressive ocean waves. Further research into the details of the numerical implementation and characterization of the wave regression functions are need in order to provide a robust application of the model to general ocean waves. Pipiras et al. (2023) also looked into this problem.

### 3. Hydrodynamic pressure based on an ARMA model

The ability to produce a hydrodynamically adequate wave surface provides a successful solution to both the problem of direct simulation and the inverse problem of determining hydrodynamic pressures at any point under the waves. Obviously, the solution of the problem is limited by the properties of the wind wave model.

The inverse problem in potential flow consists of finding velocities and wave pressures under the assumption that the wave elevation is known beforehand. Potential flow represents an inviscid, incompressible fluid flow field via a scalar velocity potential  $\varphi$ , which is described by the system of equations

$$\begin{aligned} \nabla^2 \varphi &= 0 \\ \varphi_t + \frac{1}{2} |\vec{v}|^2 + g\zeta &= -\frac{p}{\rho} \quad \text{on } z = \zeta(x, y, t), \\ D\zeta &= \nabla \varphi \cdot \vec{n} \quad \text{on } z = \zeta(x, y, t) \end{aligned} \quad (10)$$

where  $\zeta$  is the wave elevation,  $p$  is the wave pressure,  $\rho$  is the water density,  $\vec{v} = (\varphi_x, \varphi_y, \varphi_z)$  is the velocity vector,  $g$  is the gravitational acceleration and  $D$  is the substantial derivative. The first equation is the continuity equation, which along with the Navier-Stokes equations, which together form the field equations for the three velocities and the pressure in a viscous fluid — incompressible in this case. The second equation is the so-called dynamic boundary condition on the free surface. It comes from Bernoulli's equation for the pressure in an inviscid fluid, which is derived by integrating the Navier-Stokes equations along a streamline. The dynamic boundary condition requires that the pressure on the free surface be a constant (often taken a zero). The last equation is the kinematic boundary condition for the wave free surface, which states that there can be no flow across the free surface, any particle on the free surface remains on the free surface.

The classical approach to solving the surface-wave problem is to linearize the boundary conditions and their definition about  $z = 0$  (note that there is no unique linearization.), since the direct solution of the problem is difficult both due to the nonlinear boundary conditions and the unknown boundary where they are applied. In the case of solving the nonlinear problem, a sequential determination of both the velocity potential and the present shape of the wave surface is used. This is what requires the presence of two boundary conditions from a mathematical point of view. If the wave surface is known initially, then the kinematic boundary condition turns out to be linear and the Laplace equation can be solved analytically at any given moment of time. The solution to this problem is the realization of  $\varphi(x, y, z, t)$  and, consequently, all its derivatives with respect to space and time. In this case, Bernoulli's equation can be used to directly calculate the hydrodynamic pressures at any point.

The analytical solution and computational procedure for the potential flow were presented in [Degtyarev and Gankevich \(2015, 2019\)](#). [Degtyarev and Gankevich \(2019\)](#) gives an approximate solution based on the use of a local dispersion relation, which leads to a simple final expression. The exact solution of [Degtyarev and Gankevich \(2015\)](#) turns out to be more complicated, but it can also be expressed in a finite form, which makes it possible to implement a simple computational procedure.

For the two-dimensional case, the solution is as follows:

$$\varphi(x, z) = \frac{1}{2\pi i} \int_{-\infty}^{\infty} \frac{1}{\lambda} e^{\lambda(z+ix)} d\lambda \int_{-\infty}^{\infty} \frac{\zeta_t}{1 - i\zeta_x + i\zeta_x/\sqrt{1 + \zeta_x^2}} e^{-\lambda(\zeta+ix)} dx \quad (11)$$

The three-dimensional problem can be solved with the help of a special inversion formula which serves as a modified version of a Fourier transform ([Degtyarev and Gankevich, 2015](#)). In polar coordinates, the transform has the following form:

$$F(\rho, \psi) = \int_0^{\infty} \int_0^{2\pi} r f(r, \theta) e^{ir\rho \cos(\psi-\theta) + r\zeta(\rho, \psi)} d\theta dr \quad (12)$$

In this case, the final expression for the velocity potential is ([Degtyarev and Gankevich, 2015](#)):

$$\varphi(x, y, z) = \mathcal{F}^{-1} \left\{ \frac{\mathcal{F}\{\zeta_t(x, y)\} \mathcal{F}\{e^{M(iNx+\zeta)}\}}{\mathcal{F}\{f(x, y)e^{M(iNx+\zeta)}\}} \right\} \quad (13)$$

where  $\mathcal{F}$  is an ordinary forward Fourier transform, with  $M, N$  — scales of wave number and space (dimensionless transformation  $(x, y) \rightarrow (xN, yN)$ ),

$$f(x, y) = M \frac{N^2 + i\zeta_x \left( \sqrt{N^2 + \zeta_x^2 + \zeta_y^2} - N \right)}{N \sqrt{N^2 + \zeta_x^2 + \zeta_y^2}} \quad (14)$$

There is no easy way to derive an analogous formula for the derivatives of the velocity potential. However, numerical experiments have shown that there is no need to do this. These derivatives can be obtained numerically via finite difference formulae. Fewer integral transforms means less numerical error and faster computation.

From the computational point of view, the velocity potential is given by four fast Fourier transforms and velocity via three numerical differentiations (one for each coordinate), in other words its asymptotic complexity is roughly  $4n \log_2 n + 3n$ , where  $n$  is the total number of points in the volume. Successful verification of the proposed procedure is presented in [Degtyarev and Gankevich \(2015\)](#).

[Fig. 9](#) presents a slice of a wave surface generated by an autoregressive wind wave model with waves of large amplitude, and the corresponding streamlines below the surface. In the figure, the streamlines are skewed opposite to the direction of wave propagation. This hydrodynamic solution was tested against the wave surface generated by the autoregressive wind wave model and it was found that the shape of streamlines and potential field is indeed asymmetric.

This solution allows a velocity field to be determined for waves of arbitrary amplitudes and is fast from a computational point of view ([Degtyarev and Gankevich, 2019; Weems et al., 2016](#)). For plain waves, the solution gives the same field as previously known solutions and for large amplitude waves it gives an asymmetrical velocity field. Bernoulli's equation can be used to calculate incident wave pressures for the calculation external forces and moments.

$$p(x_0, y_0, z_0) = -\rho\varphi_t - \frac{\rho}{2} (\varphi_x^2 + \varphi_y^2 + \varphi_z^2) - \rho gz_0. \quad (15)$$

The efficient realization of these computations depends largely on the choice of algorithm and the way it is implemented on modern hardware. The main computational problem is the transition from the continuous analog of (10)–(14) to a discrete implementation, which is possible on a computer. This transition is especially relevant for direct simulation of hydrodynamic processes.

#### 4. Numerical construction of objects in a continuous medium

Direct simulation in continuum mechanics using discrete digital computers is based on a limited set of digital objects that interpolate the parameters of the state of the physical fields temporally. Computational processes with such numerical objects must take place in accordance with physical laws in the meshed areas (including irregular meshes). At the same time, each mesh cell is represented as an independent

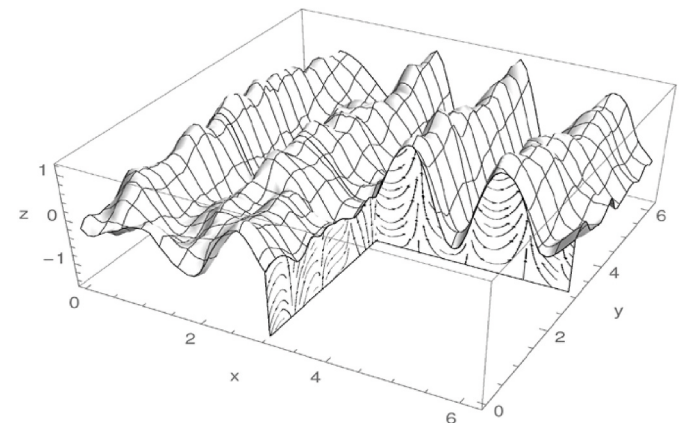


**Fig. 9.** Slice of a wavy surface with waves of large amplitude generated by autoregressive wind wave model.

corpuscle actively interacting with the surrounding particles (Khramushin, 2005).

Let us call one mesh cell an elementary computational object (large particle of continuous medium with finite volume). All internal transformations of such a particle within linear approximations is strictly and uniquely determined by the rules of tensor arithmetic. This is a convenient tool for describing the geometry and kinematics of a large particle. Apart from its position in space, classical tensor calculus describes more complex transformations: rotation, compression, elastic deformation etc. Its functional apparatus is sufficient to develop strong forward and reverse mathematical descriptions of the physical processes of fluid mechanics in the finite mesh area.

For the description of large mobile elementary particles in a three-dimensional space, we introduce two coordinate systems: absolute and moving local (associated with the particle) (Fig. 10).

Let us initially restrict our consideration to distant fluid mechanical interaction. Then the fluid mechanical laws for local interaction define global force interactions, inertial reactions and internal deformations. All the laws of fluid mechanics and the kinematics of fluid transformation are represented as linear spatiotemporal dependencies of the simplest tensor-vector form. Writing a computational algorithm in tensor notation makes implementation on a computer most efficient, especially if low-level operations on sets of numbers can be used.

For the convenience in representing analytic expressions, let us define the following notations for vector and tensor quantities in their finite-difference representations (Khramushin, 2005).

A – value measured in a global coordinate system (may only be a scalar or vector),

a – value measured in a local basis, it refers to small volume or contiguous particles only (differential differences, can be scalar, vector or tensor)

$\vec{R}, \vec{r}$  – values projected on the global basis,

$\hat{\vec{R}}, \hat{\vec{r}}$  – values projected on the local basis,

$\hat{\vec{r}}$  – local tensor in projections of global system,

$\vec{r}$  – local tensor in projections of local system.

A more detailed notation is provided in appendix 1.

With this notation, capital letters are used for values in global coordinate system. Lower letters are used for small quantities for local bases projections in spatial location and current time. The basic mathematical operations are tensor products and products of tensors and

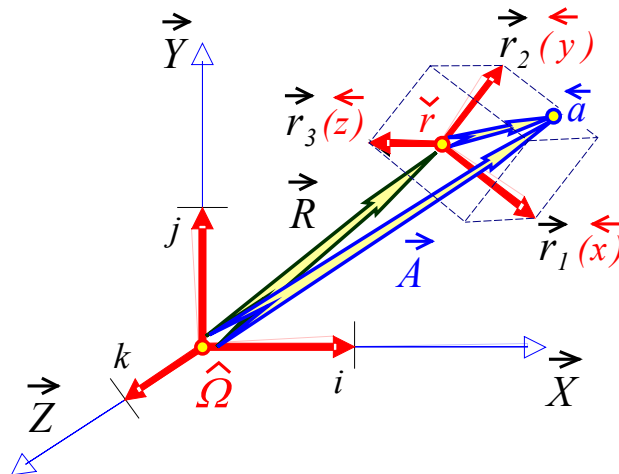


Fig. 10. Local basis  $r_i$  is formed by triad of basis vectors,  $ijk$  – unit vectors of global coordinate system (XYZ);  $R$  – radius vector of the moving system;  $A$  – radius vector of the point in global coordinate system;  $\vec{a}$  – the same point in local coordinate system.

vectors. They define the ratio of local reactions of fluid particles to the external influence of the environment. The formal possibility of rank increasing tensor-vector objects is excluded. They have no immediate physical interpretation.

The absolute or full velocity vector of a large particle is introduced as a shift of the center of mass in the global coordinate system:

$$\vec{V} \cdot t = {}^A\vec{R} = {}^t\vec{R} = {}^0\vec{R} = {}^T - {}^t\vec{R} = {}^T\vec{R} \quad (16)$$

A tensor of the instantaneous velocities relative to the nominal center of a large particle projected on the absolute coordinate system is assembled by direct geometric constructions. Obviously, such a tensor contains the components of rotation and the velocity of mutual deformation of the basis vectors of the adjacent points in the fluid flow:

$$\hat{\vec{v}} = \vec{v}^i = {}_A\vec{V}_i = {}_+ \vec{V}_i - {}_\Omega \vec{V}_i \quad (17)$$

At the initial instant, the tensor internal flow velocities equal to zero. This is acceptable in the Euler stages of the simulation.

The kinematics of the internal flows of elementary fluid particles is algorithmically constructed as differential velocity tensors (Fig. 11). This is a tensor of basis vector form for large fluid particles moving in time:

$$\hat{\vec{v}} \cdot t = \vec{v}^i \cdot t = {}_A\vec{r}_i = {}_+ \vec{r}_i - {}_\Omega \vec{r}_i [\text{m}^3] \quad (18)$$

Tensor  $\hat{\vec{v}}$  sets the current velocity of the unit vectors in the local basis (lower case) with respect to the global coordinate system (subscripts). For local analysis it can be transferred to the local reference system (normalization of geometric measurements):

$$\nu \geq \hat{\vec{v}} \cdot \hat{\vec{r}} = \hat{\vec{v}} / \hat{\vec{r}} [\text{s}^{-1}] \quad (19)$$

Here the known tensor of convective velocities is formed automatically. The traditional definition of an affinor, i.e. affine tensor of type (1,1), (high-order tensor) is applicable to it and the theorem of Helmholtz (Lamb, 1975) for the decomposition in small increments of time is reasonable: expansion (divergence); turn (rotation) and deformation (shift).

## 5. Definition of space operations over the elementary particles of a fluid

Computing objects are created at the initial formation of the hydrodynamic fields in the mesh area. The mesh area is dynamically changeable and irregular, depending on the current regimes in the local area and the features of the problem. These objects are constructed immediately during the computing experiment. Their appearance is the result of special logical procedures that control specific regimes of the fluid flow and the progress of the simulation on a functional level. A striking example of such procedure is the change of mesh area in zones

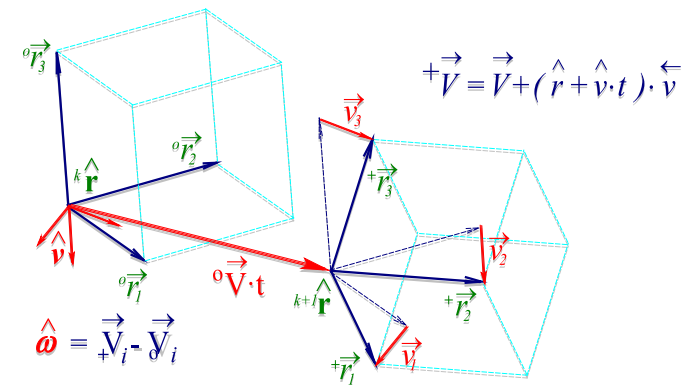


Fig. 11. Tensor of local velocities formed by the deformation displacements of the basis vectors of large fluid particles for the time interval.

of cavitation and vortex break-up and also on free surfaces. Computing objects cannot be generated or destroyed as a result of mathematical manipulations (generation of vector dyads or tensors of the third rank are excluded by the logic of the creation of computing objects) (Degtyarev and Khramushin, 2014).

Control of the physical state of objects (large particles) allows determination of the type of computing operations dynamically. To correctly carrying out direct simulation, it is necessary to meet the following requirements in the mathematical models:

1. Elementary spatiotemporal objects and the basic physical phenomena must be described in dimensional form.
2. Physical properties of the environmental and fluid mechanics laws for the modeled phenomena are formulated in canonical form. The transition to a required reference systems is carried out automatically at the algorithmic level.
3. Properties of arithmetic operations and elementary numerical objects are invariantly defined in the global coordinate system and correspond to calculated values in the local basis. This is carried out by multiplication operations.

Taking into account the history of the movement, "confined" fluid particles are governed by the vector analog of Newton's law (Zommerfeld, 1954). (Fig. 12)

$$W_i = F_j \cdot M_i^j \text{ or } \vec{W} = \vec{F} \cdot \vec{M} \quad (20)$$

$${}^+ A_x = {}^0 A_x + (V_x + \alpha^x v_{xx} + \alpha^y v_{yx} + \alpha^z v_{zx}) ; {}^+ A_y = {}^0 A_y + (V_y + \alpha^x v_{xy} + \alpha^y v_{yy} + \alpha^z v_{zy}) ; {}^+ A_z = {}^0 A_z + (V_z + \alpha^x v_{xz} + \alpha^y v_{yz} + \alpha^z v_{zz}) .$$

where the external force  $\vec{F}$  affects the large fluid particles within the stream  $\vec{M}$  and causes reaction  $\vec{W}$ . The  $\times$  icon above the letters in Fig. 12 means that it can be both  $\wedge$  and  $\vee$ . The value and direction of  $\vec{W}$  depends on both the internal state (inertia) of this particle, and on its ability to be deformed, to absorb or to strengthen external manifestations of motion

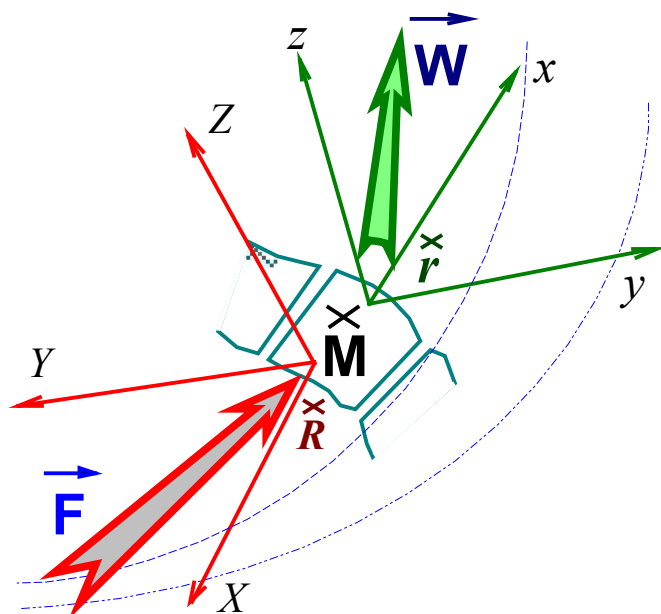


Fig. 12. Large particle in the process of motion and deformation.

energy. Linking the mass tensor with the fluid particles  $\hat{M} = \hat{r} \cdot \hat{\rho}$ , we obtain the definition of density or internal energy, which corresponds to the anisotropic properties of the fluid environment:

$$\vec{F} = r_{ik} \cdot \rho^{kj} \cdot \vec{W} = \hat{r} \cdot \hat{\rho} \cdot \hat{W} \quad (21)$$

where  $\hat{r}$  [ $m^3$ ] is the tensor of a large fluid particle;  $[kg/m^3]$  is the density tensor characterizing the internal state of the fluid particle, taking into account the dynamic interaction with the continuous medium.

Small spatial movements are determined by the changes in the flow underlying Newtonian mechanics. In kinematic problems, the variation in the flow determines the velocity-determining differential (by Newton – the moment) as a product with a given time step.

Within such views, large particle kinematics is given by the differential (moment) of velocities in the absolute coordinate system, subject to small displacements in the local basis:

$${}^+ \vec{A} = \vec{R} + \vec{V} \cdot t + \vec{Z}, \quad (22)$$

where  $t$  is calculated time moment;  $\vec{a}$  is coordinates of the control point (see Fig. 10) in the local reference system;  $\vec{R}$  is the location of the local basis in the absolute coordinate system;  $\vec{v}$  is the speed of forward shift of the local basis (of large fluid particle);  $\vec{z}$  may have a different form depending on the mode of the current. In the simplest case  $\vec{Z} = \vec{a} \cdot (\hat{r} + \hat{v} \cdot t)$ . We then represent (22) as  ${}^+ \vec{A} = {}^0 \vec{A} + (\vec{V} + \vec{a} \cdot \hat{v}) \cdot t$  or in the form of a system of scalar equations (Kochin, 1965):

In case of vortex flow, in accordance with the Cauchy-Helmholtz theorem (Zommerfeld, 1954)  ${}^+ \vec{A} = \vec{R} + \vec{V} \cdot t + \vec{a} \cdot (\hat{r} + \hat{v} \cdot t) + \vec{\omega} \cdot (\hat{r} + \hat{v} \cdot t) \cdot t$ . Here  ${}^+ \vec{A}$  and  ${}^0 \vec{A}$  are new and initial locations of a control point in the global system;  $\hat{r}$  is a tensor of large fluid particle form;  $\hat{v}$  is a tensor of the speeds of local motions of the basic axes of the tensor defining the deformation of a large fluid particle;  $\vec{\omega}$  is the speed of internal shift.

Let us present the equation for the motion of an arbitrary point (22) near a large fluid particle in a convenient dynamic form. Here we take into account deformation and energy of internal forces:  $\hat{m}$  [ $kg^{-1}$ ]. We have to consider varying nature of such: external distributed forces  $\hat{f}$  [ $N/m^2, kg\ m^3/s^2$ ] and mass  $\vec{F}$  [ $N, kg\ m/s^2$ ]:

$${}^+ \vec{A} = \vec{R} + \vec{V} \cdot t + \hat{m} \cdot \vec{F} \cdot t^2 / 2 + (\hat{r} + \hat{v} \cdot t + \hat{m} \cdot \hat{f} \cdot t^2 / 2) \cdot \vec{a}, \quad (23)$$

The resulting expression contains the traditional system of Euler's equations of fluid mechanics and an additional term describing the deformation of a large fluid particle under the influence of the stress on its boundaries.

## 6. Algorithmic realization of the hydrodynamic laws

The algorithmic implementation is based on a computational scheme using a mixed Lagrangian-Eulerian approach (Lamb, 1975; Degtyarev and Khramushin, 2014). This is similar to the methods of "large particles" (Belocerkovski and Davidov, 1982) and "final volume" (Patankar, 1991) for the double integration of the first order equations of motion. Thus, the time cycle of computing the simulation is divided into three notional stages:

Stage 1 – Kinematic parameters are calculated for the centers of the large fluid particles. For this purpose, the instantaneous data at fixed nodes of the Eulerian coordinates are used;

Stage 2 – Lagrangian, large deformable fluid particles are in free motion. They redistribute the internal properties of the original Euler cells to adjacent cells;

Stage 3 – Laws of conservation of mass and energy are enforced consistently. This is achieved by deformation of the shifted fluid particles. The next step is the re-interpolation of the characteristics of present solution to the initial nodes of the fixed Euler computational mesh.

The computational simulation is generally presented as an integral transformation of the velocity field in absolute time:

$$+ \vec{V} = \vec{V} + \vec{W} \cdot t, \quad (24)$$

Thus, the construction of the computational experiment is reduced to a difference derivation of the first order. This is the main feature of the Lagrangian-Eulerian approach for the numerical solution of problems in fluid mechanics. In other words, it is possible to consider this approach a method for splitting the physical processes, which can be formed by three nominal stages of the numerical solution of applied problem:

*Stage 1.* Based on the current velocity field, the state of large fluid particles in the following instant is specified:

$$+ \hat{M} = \hat{\rho} \cdot \hat{r} + \hat{v} \cdot t, \quad (25)$$

where  $\hat{v}$  is the tensor map of the current velocity field on the local basis of a large particle;  $\hat{\rho}$  is the  $\hat{\rho}$  tensor of the internal state of a fluid particle at the current instant of time.

*Stage 2.* After the specification of the resultant vector of all external forces acting on a large fluid particle, calculation of new velocity field is carried out:

$$+ \vec{V} = \vec{V} + \hat{M}^{-1} \cdot \vec{F} \cdot t, \quad (26)$$

*Stage 3.* The first two phases result in the spatial displacement of the large fluid particles. The new hydrodynamic fields no longer completely satisfy the conditions of continuity nor provide an isotropic environment. Depending on the type of problem, a final stage is necessary to relax the absolute properties and interaction conditions between the fluid particles. It is necessary to carry out a walkthrough to control of the quality of the solution. We must, if necessary, apply a scheme of adaptation or empirical amendment of the solution in areas where the computational model gives a clearly incorrect result.

It is known that traditional approaches to the numerical solution of fluid dynamics problems are often reduced to the application of implicit schemes (Alder et al., 1964; Pletcher et al., 2013). The algorithmic approach is described first of all because of the proposed splitting of the solution based on physical processes, provides an opportunity to apply explicit numerical schemes to the first two stages. In this case it is possible to increase the effectiveness of computing procedures through:

1. Natural parallelization of the computation process;
2. Possibilities of adaptive correction of mesh area depending on the features of the problem;
3. Dynamic reconstruction of the solution in accordance with fluid flow transformations in time.

This approach allows for the efficient design of computational algorithms for direct simulation of ship behavior in waves. The tensor

form for recording the state of the system provides a natural mapping of the algorithm to the computer architecture, since it strictly defines the relationship between the continuous and discrete analog of the problem under consideration. Let us next consider its implementation in the direct simulation of ship dynamics in waves.

## 7. Computational algorithms for a trochoidal wave model

In this paper, a numerical model using trochoidal waves is developed in addition to the ARMA model. It focuses on the instantaneous velocities and trajectories of fluid particles that create an impulsive force on the ship's hull. Very strong drift currents are formed on the excited sea surface. Formally, such equations universally satisfy the continuity condition, which is more consistent with the objectives of direct simulation. Real storm sea wave conditions are reproduced, including the case of a notional wave group of nine waves. — the middle wave of a "three sisters" encounter.

The mathematical model of trochoidal waves  $\vec{\zeta}(t, s, z)$  [m] is written in vector form (vector of displacement of particles in the vertical plane) on the wave profile plane  $w \in \{s, z\}$  in the direction of wave front propagation  $s$  [m] with  $z$  [m] vertical (Degtyarev et al., 2020). For direct simulation purposes, the model is for brevity written using finite differences. This is preceded by an analysis of the stability of the computational processes in time and a preliminary adjustment of the smoothness of the approximated hydrodynamic fields. This is expressed in the form of C programming language operations:  $x+ =$ ,  $x- =$ , etc.).

The boundary around the rectangular calculation region pre-determines the wave half-height by means of the trochoidal radius  $r_w$  [m] at the level of the undisturbed sea surface  $z = 0$  [m]. Based on this radius, the orbital motion of each elementary particle depends on its instantaneous depth beneath the water surface  $r_z$  [m]:

$$r_z \times = \exp(2\pi \cdot z / \lambda) \text{ [m].} \quad (27)$$

In algorithmic models of wave processes, it is convenient to use the coefficient:  $H_w = 8/3 \cdot \pi \cdot h / \lambda$ , normalized with respect to the maximum allowable height of a breaking trochoidal waves. Here  $h = 2 \cdot r_w$  [m] is the limiting wave height — the doubled radius of the surface trochoid.

We assume that fluid particles move along their own trochoidal trajectories below the water surface. Water pressure is determined by the depth and local velocity of the particles under the wave profile. A symmetric correction with respect to the wave phase  $Cr \approx [0 \div H_w \div 1]$  to the local depth  $r_z$ , partially compensates for the loss of fluid volume during the formation of the pointed tops of the cnoidal waves:

$$r_z \times = \exp(2\pi \cdot r_z \cdot Cr \cdot \cos \varphi_w / \lambda) \text{ [m],} \quad (28)$$

If necessary, an additional asymmetric correction to the wave profile is introduced to account for wind stresses:  $Wd [0 \div \sqrt{0,5} \div \sqrt{0,5} \div 1]$ :

$$r_z \times = \exp(2\pi \cdot r_z \cdot Wd \cdot (\sin \varphi_w - 1) / \lambda) \text{ [m],} \quad (29)$$

It can be applied exclusively to wind waves with an average significant shear, as:  $Wd \approx \sqrt{0,5} \approx 0,7071$ .

Wave group structures form rhombic cells with extension in the direction of crest spreading:  $L_g = \lambda \cdot 8.89$  [m]. The largest front extension, the width of a rhombic water cell, is  $F_g = 2\pi \cdot \lambda / H_w$  [m] so it is inversely proportional to the relative height of the ninth wave in the center of the wave group structure.

The actual profile of the mathematical surface-wave model is constructed in vector form based on the local radius  $r_z$ , applied to the simple harmonic displacement of water particles from their initial neutral position:

$$\vec{\zeta} + = r_z \{ -\cos \varphi_w, \sin \varphi_w \} \text{ [m]} \quad (30)$$

In a gravity wave, the fluid particles move along trochoidal orbits with strictly equal angular velocities:  $V_r = \omega \cdot r_z$  [m/s], which determines the

phase velocity of the free motion of a progressive wave crest:  $C_w = \lambda/\tau = \omega/k$  [m/s]. The immersion of the fluid particle is measured from the level of the actual wave surface. Trochoid radii and curvature of particle trajectories are scaled to the geometric proportion of the trochoidal wave as a whole (27) and (28):

$$V_r = \omega \cdot r_z = \omega \cdot r_w \cdot e^{kz}$$

or for the sea surface:

$$V_w = \omega \cdot r_w \exp(2\pi/\lambda \cdot (z + r_w(\sin\varphi - 1))), \text{ [m/s]} \quad (31)$$

where  $z$  is in the global Cartesian reference system.

To construct the visual kinematics of trochoidal wave profiles with dispersion, we use the operator for the doubled rotation of the calculated fluid particles (calculated points on the wave profiles of trochoidal radii  $\vec{\zeta} \cdot \text{curl}(\omega t)$ ). Group velocity  $U$  must be used in the calculations instead of the phase velocity  $C_w$ . By analogy, in the case of capillary waves, the dispersion relation agrees by a simple change of sign in front of the circular velocity  $\vec{\zeta} \cdot \text{curl}(-\omega t/2)$ . Depending on the nature of the waves being visualized, its phase shift varies. For waves in deep water we have a positive increment of the phase angle  $\varphi_w + = \omega \cdot t$ . Capillary wave kinematics are provided by the following phase retardation:  $\varphi_w - = \omega \cdot t/2$ .

For direct simulation purposes, the model is written using finite differences. This is preceded by an analysis of the stability of computational processes in the time domain and a preliminary assessment of the approximation smoothness of the simulated hydrodynamic fields.

The three-dimensional velocity distribution of flow is quite correctly modeled using wave hyperbolic equations. Boundary conditions and approximation criteria are well developed for them, including in conditions of application of empirical engineering approximations.

The stability of the solution of the wave equation is controlled quite reliably by the use of the Courant criteria, the essence of which is to prevent the intersection of the perturbations of the simulated computational cells as a whole during one computational time-step.

$$C_w < \delta s/\delta t, \quad (32)$$

where  $C_w$  [m/s] is the given phase velocity of the simulated wave;  $\delta s$  [m] is the mesh step size which is the same in the entire computational domain;  $\delta t$  [s] is the time step for one cycle of the computational experiment.

Fig. 13 shows trochoidal wave flow trajectories, illustrating the dependence of drift currents on the depth of the fluid particles and the relative height of the wave crests. The maximum velocity of the surface flow is reached on the crest of a breaking progressive wave, where its magnitude can approach the phase velocity of a single wave. The grid below the wave crest illustrates the drift displacement of particles and lines of equal pressure below the surface of the wave. The quasi-trochoidal trajectories of the fluid particles in motion above the wave with, fixed angular velocities determines the phase velocity of the wave.

The theory of trochoidal waves contains a visual interpretation of the computational processes using the motion of fluid particles in moving Lagrangian coordinates, which naturally appears in the corpuscular stage of a direct computational experiment. Drift flow in the upper layers of the fluid is modeled by changing the curvature of the particle trajectory as a function of the instantaneous level change in the wave profile. Thus, the computational model initially provides for consideration of unsteady hydromechanics of a ship in a stormy sea.

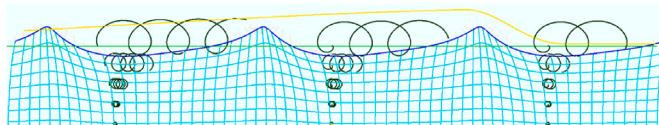


Fig. 13. Modeling of regular trochoidal waves under the action of surface wind and correction for the shift of mean sea-level.

Computational resources of modern computers are quite sufficient for realization of direct computational experiments in real time on board a ship in the open sea, which can be demanded when choosing optimal and effective modes of storm navigation.

Time step  $\delta t$  needs to be slightly reduced compared to Courant condition  $\delta t < \delta s/C_w$ , to achieve stable solution. Factor of  $tKrat \approx \sqrt{2}$  is used for rectangular grid. Another empirical correction to time step is needed for correct modeling of radiation, i.e. Sommerfeld radiation conditions. This correction is introduced for the normal component of the radiated wave as a factor  $tK = tKrat/(tKrat + 1)$ .

To simplify the algorithmic notation, a dimensionless wave parameter is introduced  $kW = \frac{C_w}{tKrat} \frac{\delta t}{\delta s}$ , which is the ratio of the wave celerity and the maximum allowable velocity of the wave passing through a cell, i.e. the wave front would not pass the cell over one time step.

Extrapolation conditions according to Sommerfeld are defined at free boundaries for undamped radiation of progressive waves with a pre-determined phase velocity  $C_w$ . They are used in calculations of the displacement of the normal slope component of the radiating wave:

$$\begin{aligned} \vec{\zeta}_+ &= kW \cdot (\vec{\zeta}_0 - \vec{\zeta}) \cdot tK = C_w \frac{\delta t \cdot (\vec{\zeta}_0 - \vec{\zeta})}{\delta s \cdot (tKrat + 1)} \quad [\text{m}], \\ \vec{\zeta}_+ &= kW \cdot (\vec{\zeta}_{n-1} - \vec{\zeta}_n) \cdot tK = C_w \frac{\delta t \cdot (\vec{\zeta}_{n-1} - \vec{\zeta}_n)}{\delta s \cdot (tKrat + 1)} \end{aligned} \quad (33)$$

where lower left indexes 0,  $n$  are used to mark the grid nodes; the symbol (+) as a left upper index shows the next time instant.

The dynamics of the fluid particles is plotted in the vertical plane of the wave profile, where the grid differences separated by half a spatial step provide synchronous interaction of the displacement vectors of the fluid particles  $\vec{\zeta}$  [m] with their local velocities  $\vec{\nu}$  [m/s] referenced to the phase velocity of the wave propagation  $C_w$  [m/s] and the angular rotation of the constituent particles  $\omega$  [1/s]:

$$\begin{aligned} \vec{\zeta}_- &= kW \left( \vec{\nu}_s - \vec{\nu}_{s-1} \right) / \omega = C_w \frac{\delta t \cdot (\vec{\nu}_s - \vec{\nu}_{s-1})}{\delta s \cdot tKrat} / \omega \quad [\text{m}] \quad \{s \in 1 \dots n-1\} \\ \vec{\nu}_s &= kW \left( \vec{\zeta}_{s+1} - \vec{\zeta}_s \right) \cdot \omega = C_w \frac{\delta t \cdot (\vec{\zeta}_{s+1} - \vec{\zeta}_s)}{\delta s \cdot tKrat} \cdot \omega \quad [\text{m/s}] \quad \{s \in 1 \dots n\} \end{aligned} \quad (34)$$

where at the end knots with variations in the level and drift of the fluid particles, the  $\vec{\zeta}_+$  are extrapolated from the instantaneous fields with boundary conditions (33).

The dispersive effects of trochoidal waves are evident when considering the rotation  $\omega_z$  of fluid particles relative to the centers of trochoidal radii. rotation  $+ \omega$ , a doubled phase velocity with respect to the propagation velocity of the wave packets is simulated. When the sign of  $- \omega$  is reversed, the group velocity increases by a factor of 1.5 relative to the apparent velocity of the wave fronts. This is characteristic of capillary (surface tension) waves. In both cases of the influence of dispersion, the phase of the arrival of the first wave at the wave front at the undisturbed water changes visually:

$$\begin{aligned} \vec{\zeta}_- &= \delta t \omega \{ -\zeta_z + \zeta_x \cdot \delta t \cdot \omega/2, \zeta_x + \zeta_z \cdot \delta t \cdot \omega/2 \} \\ \vec{\nu}_s &= \delta t \omega \{ -\nu_z + \nu_x \cdot \delta t \cdot \omega/2, \nu_x + \nu_z \cdot \delta t \cdot \omega/2 \} \end{aligned} \quad (35)$$

Trochoidal wave theory enables visual interpretation of the computational processes through tracking the motion of fluid particles in the moving Lagrangian coordinates. This is naturally presented at the particle stage of a direct simulation, by using the numerical methods of tensor mathematics, the large-particle method. The drift flow in the upper fluid layers is modeled by the changing curvature of the particle trajectories, which depend on the instantaneous level change in the wave profile.

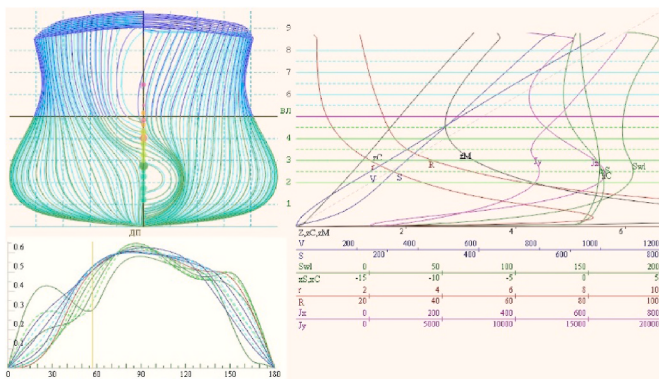


**Fig. 14.** Visualization of the hydrostatic characteristics of the hull and ship stability. On the left, the hull projection shows stability curves at different drafts for zero metacentric height at fixed center of gravity, which corresponds to the real dynamics of the ship under storm conditions. In the center is a set of hydrostatic curves for all drafts from keel to deck.

The main result obtained in this paragraph is that a way to simulate a physically real free wave surface is proposed. This means that the realization of such a wind wave can be used a direct computational experiment. Thus, the computational model initially provides for the non-stationary hydrodynamics of a ship in heavy seas. The computational resources of modern computers are quite sufficient for the implementation of direct, real-time computational experiments on board a ship at sea, which can be required when choosing optimal and efficient navigation routes in storm conditions.

## 8. Geometrical objects and operations for ship hull representation

The computational experiment is built through the solution of independent physical processes, which makes it possible to interactively control the parameters of the ocean waves and the nature of the ship-wave interaction forces. The control of ship speed and course in severe seas is carried out using differential extrapolations to obtain smooth kinematics of the vessel under the control of dynamically similar thrusters and rudders.

The numerical model of the moving ship interacts separately with each of the basic wave structures, correctly reproducing the main hydrodynamic effects of the diffraction of trochoidal waves by the ship's hull. The resulting wave field and the spatial distribution of the subsurface flow velocities are obtained by vector summation (a simple superposition) of independent trochoidal wave processes, and serves to calculate the hydrodynamic forces and reactions of the general impact of storm wave crests, in general, determining the storm hydromechanics of the ship with a changing arbitrary courses relative to the waves.

Computations are accelerated by use of spatially ordered numerical structures to describe the ship hull surfaces, which also makes it possible

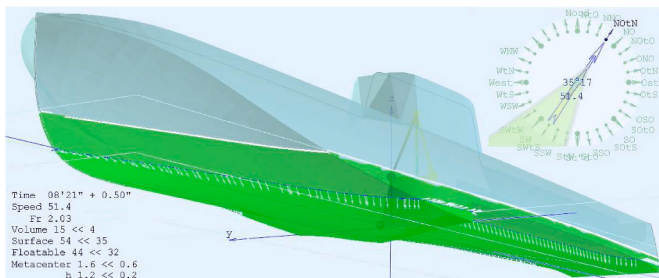
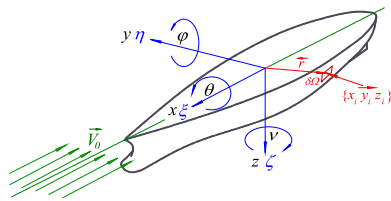


**Fig. 15.** Numerical simulation of a high-speed planing boat on calm water. At 50 knots ( $F_n = 2$ ), ship displacement reduces from  $15 \text{ m}^3$  to  $4 \text{ m}^3$ , wetted surface reduces from  $44 \text{ m}^2$  to  $32 \text{ m}^2$ .

to include re-enterable algorithms for parallelizing the entire computation process. At each step of the experiment, the intersection points of the wave slopes are re-interpolated and beamlines are placed for dynamic construction of the waterline with the separation of the underwater and above water hull volumes. New volumes with displaced centers of buoyancy (moments of inertia) are calculated from the underwater contours. The integral direction of hydrostatic forces is averaged using the gradients of the wave surface slope gradients.

The metacentric characteristics of the hull are computed in the simulation process, but they are used only for visual control of the ship dynamics in traditional ship motion theory (Fig. 14). For this purpose waterplane area, centroid of the instantaneous waterplane and the moments of inertia of the waterplane, metacentric radii and the vertical position of the metacenters from the instantaneous center of buoyancy are also calculated (see Fig. 15).

Volume [ $\text{m}^3$ ] and Surface [ $\text{m}^2$ ] are the displacement and wetted surface of ship hull in calm water;  $iV$  [ $\text{m}^3$ ] is the submerged volume of the ship hull with motion in waves;  $\overrightarrow{\text{Buoyancy}}$  and  $\overleftarrow{\text{V}}$  [ $\text{m}$ ] are the centers of buoyancy in still water and waves;  $\gamma \overrightarrow{\text{B}} = g \cdot \rho \cdot \overrightarrow{B}$  [ $\text{kg} \cdot \text{m}/\text{s}^2$ ] is the vector of buoyant forces;  $\overrightarrow{\text{Floatable}}$  and  $\overleftarrow{\text{V}}F$  [ $\text{m}$ ] are centers of waterline area in still water and waves;  $\overrightarrow{vW}$  [ $\delta$ ] is the normal vector to the wave surface;  $\overrightarrow{vS}$  [ $\text{N}/\rho$ ] and  $\overrightarrow{vR}$  [ $\text{N} \cdot \text{m}/\rho$ ] are vectors of forces and moments at elementary ship hull surface patches taking into account the pressure reduction in accordance with Bernoulli law:  $\delta h_z = 0.5 \cdot (\delta V)^2/g$  [ $\text{m}$ ].



$\overrightarrow{G} \{ \xi, \eta, \zeta \}$  (x-surge, y-sway, z-heavy)[M] are the coordinates of the center of gravity in the moving ship coordinate system;  $\overrightarrow{\Omega} \{ \theta, \psi, \nu \}$  (x-roll, y-pitch, z-yaw) [ $^\circ$ ] are angular coordinates: roll, pitch and yaw;  $\overrightarrow{V}$  [ $\text{m}/\text{s}$ ] is the vector of translational velocity and  $\overrightarrow{\omega}$  [ $^\circ/\text{s}$ ] is the vector of angular velocity;  $\overrightarrow{r}$  [ $\delta^3$ ] is ship basis as a dimensionless normalized tensor of rotation;  $\rho \cdot \text{inMass}$  [ $\text{kg} \cdot \text{m}^2$ ] is the mass (volume [ $\text{m}^3$ ]) tensor of ship inertia;  $\overrightarrow{L}$  [ $\text{m}$ ] – shoulder of divergence of centers of buoyancy and gravity.

Each of these objects is described either in a fixed global coordinate system — with definition in capital letters, or in a local reference system fixed to the ship — with lowercase entries. Vector quantities can be measured in the local ship basis with the arrow to the left  $\overleftarrow{a}$ , or in global fixed marine coordinate system with the arrow to the right  $\overrightarrow{A}$ .

Projections of free vectors are related by product operations with an orthogonal, orthonormal ship basis tensor (orientation tensor)  $\overrightarrow{r} = \overleftarrow{r} = \overleftarrow{r}^T$ :

$$\overrightarrow{A} = \overrightarrow{r} \cdot \overleftarrow{a} - \text{from ship (local) basis to global coordinate system};$$

$\overleftarrow{a} = \overrightarrow{A} / \overrightarrow{r}$  – return of free space vector to orientation relative local basis. Accordingly, a complete recalculation of the position-related  $\overrightarrow{R}$  vectors in local and global coordinate systems are the following:

$$\overrightarrow{A} = \overrightarrow{R} + \overrightarrow{r} \cdot \overleftarrow{a} - \text{transition from local to global coordinate system};$$

$\overleftarrow{a} = (\overrightarrow{R} - \overrightarrow{A}) / \overrightarrow{r}$  back to the moving ship basis (ship) coordinate system.

which is true both for location vectors and rigid-body velocity vectors, and for angular vectors and rotational velocities.

The hull is built in the ship coordinate system with the center of

reference being the midships section at the design waterline. The main algorithm implements a sequential selection of all triangles with vertices  $\vec{a}, \vec{b}, \vec{c}$  on the hull surface, divided into three calculation stages: submerged volume, then the instantaneous waterline, and finally for visualization of the freeboard with a generalized superstructure.

The normal with area of a triangular hull surface element is:

$$\vec{S} = (\vec{a} - \vec{c}) \times (\vec{b} - \vec{c}) / 2, \quad [m^2]$$

The area of this triangle is  $W = |\vec{S}|$ .

The center of volume of the elementary tetrahedron of a surface element relative to the common center at the design waterline and midships is:

$$\vec{M} = (\vec{a} + \vec{b} + \vec{c}) / 4, \quad [m]$$

where its volume is given by scalar (dot) product:

$$V = \vec{c} \cdot \vec{S} / 3. \quad [m^3]$$

After defining the characteristic of all of the elements on the entire ship's surface, the geometric characteristics of the entire hull are calculated. The wetted surface area, submerged volume of the hull (volumetric displacement) and ship's coordinates of the center of buoyancy are the following:

$$\text{Wetted area: Surface} \sim iS = \sum |\vec{S}| = \sum_{\Delta} \frac{(\vec{a} - \vec{c}) \times (\vec{b} - \vec{c})}{2}; \quad [m^2].$$

$$\text{Displacement: Volume} \sim iV = \sum_{\Delta} \frac{\vec{S} \cdot \vec{c}}{3}; \quad [m^3].$$

$$\text{Center of buoyancy: Buoyancy} \sim \vec{vB} = \sum_{\Delta} \frac{(\vec{a} + \vec{b} + \vec{c}) \cdot [(\vec{a} - \vec{c}) \times (\vec{b} - \vec{c})] \cdot \vec{c}}{24 \cdot V}, \quad [m].$$

where  $\vec{a}, \vec{b}, \vec{c}$  are three corners of triangle  $\Delta$ .

The instantaneous waterline area  $iF$  and integral vector of the normal to water surface  $\nu \vec{W}$  of the instantaneous waterplane are:

$$iF = \sum W; \quad \nu \vec{W} = \frac{\sum \vec{S}}{iF}$$

Translational accelerations in ship motion are related to the inertial reactions of the hull mass, while the angular components of roll are related to the mass inertia tensor.

The inertia tensor for the mass of the hull is calculated from the tetrahedrons with faces on the ship's surface, all having common vertices at the origin the ship's coordinate system at amidships and the design waterline:

$$\begin{aligned} J_{xx} &= ax^2 + by^2 + cz^2 + az^2 + bz^2 + cx^2 + +ay \cdot by + ay \cdot cy + by \cdot cy + az \cdot bz + az \cdot cz + bz \cdot cz; \\ J_{yy} &= ax^2 + bx^2 + cx^2 + az^2 + bz^2 + cy^2 + +ax \cdot bx + ax \cdot cx + bx \cdot cx + az \cdot bz + az \cdot cz + bz \cdot cz; \\ J_{zz} &= ax^2 + bx^2 + cx^2 + ay^2 + by^2 + cy^2 + +ax \cdot bx + ax \cdot cx + bx \cdot cx + ay \cdot by + ay \cdot cy + by \cdot cy; \end{aligned}$$

$$\begin{aligned} J_{xy} &= J_{yx} = (2 \cdot ax \cdot ay + 2 \cdot bx \cdot by + 2 \cdot cx \cdot cy + +ax \cdot by + ax \cdot cy + bx \cdot cy + ay \cdot bx + ay \cdot cx + by \cdot cx) / -2; \\ J_{xz} &= J_{zx} = (2 \cdot ax \cdot az + 2 \cdot bx \cdot bz + 2 \cdot cx \cdot cz + +ax \cdot bz + ax \cdot cz + bx \cdot cz + az \cdot bx + az \cdot cx + bz \cdot cx) / -2; \\ J_{yz} &= J_{zy} = (2 \cdot ay \cdot az + 2 \cdot by \cdot bz + 2 \cdot cy \cdot cz + +ay \cdot bz + ay \cdot cz + by \cdot cz + az \cdot by + az \cdot cy + bz \cdot cy) / -2; \end{aligned}$$

$$\text{inMass} = \frac{\rho}{10} \int \delta V = \frac{\rho}{10} \cdot \sum \vec{J} \cdot \vec{V} \quad [\text{kg} \cdot \text{m}^2].$$

In practice, the inertia tensor should refer to the distribution of

masses of the hull structure, cargo, fuel and onboard equipment. For the estimated formalization of the characteristics of various ships and vessels, a notional distribution of masses is accepted, based on the hull uniformly filled with water, followed by a shift to a specially determined center of mass of the ship using the Steiner theorem:

$$J_{ij} = I_{ij} + \rho \cdot V \cdot (L^2 \delta_{ij} - R_i R_j)$$

where  $L \{x, y, z\} = \vec{G}$  is the vector shift axes of the rotation from the center of gravity,  $\delta_{ij}$  is identity matrix.

Volume integrals on the ship hull or surface integrals over gradient vectors of pressure (and stress) on ship hull surface are used to simulate ship hydrodynamics in large waves. External wave action is reduced to the center of buoyancy  $\vec{vB}$  relative to ship basis. Inertial and mass reactions are shifted to the center of gravity  $\vec{G}$ .

After the first preparatory steps for the simulation, the results of the still-water calculations are reassigned to the original numerical objects:

$\text{Floatage} = iF, \text{Surface} = iS, \text{Volume} = iV, \text{inMass} = \vec{m} \text{ M}$  et al. to fix the geometric, inertial and hydrostatic parameters of the ship at its static position in calm water.

A moving ship is a complex conglomeration of a conventional rigid body with its dynamic center of gravity, surrounded by dense water with a geometric center of buoyancy. In this case, the arm of reactive forces should be based on a center of lateral resistance. For the actual instantaneous immersed surface of a ship's hull in conditions of extreme ocean waves, it is determined by very complicated hydrostatic dependences.

## 9. Ship dynamics in waves

The results obtained earlier and the representation of both the vessel's hull and the equations of motion in tensor form make it possible to construct an effective computational procedure for direct simulation of the behavior of a vessel in extreme seas. The solution of the potential flow wave problem makes it possible to find the induced velocity potential, and hence the velocity of fluid particles at any point below the surface. To find the hydrodynamic pressures at these points, it is correct to apply Bernoulli's law. Then the perturbing force and moment can be found by integrating the pressures over the surface of the ship's wetted surface:

$$\vec{F} = - \int p \cdot \vec{n} \, ds$$

$$\vec{M} = \left[ \vec{L} \times \vec{F} \right]$$

where  $\vec{L}$  is the vector distance of the center of mass from the center of the underwater volume — as the point of application of the total force, or in case of hydrodynamic calculation over the whole hull surface:

$$\vec{M} = - \int p (\vec{r} \times \vec{n}) \, dS$$

where  $\vec{r}$  is the radius-vector of the element  $dS$  relative to the center of gravity.

The vector-tensor representation of the ship's hull makes it easy to calculate the integration nodes on the ship's hull and the direction of the local normal. This makes it possible to create a computationally efficient procedure.

The computational experiment is formed by applying a sequence of algorithms using vector and tensor quantities. Integration over the surface of the instantaneous wetted surface of the ship is replaced by summation using the properties of vector quantities.

Each step of the ship in time is tracked using a sequence (array) of vector samples, which, if necessary, are easily used to refine the local dynamic parameters of the ship's movement:

- Route* – ship's run — ship's instantaneous position [m];
- Rate* – ship's velocity in the ship-fixed coordinate system [m/s];
- Swing* – instantaneous values of roll, pitch yaw [rad];
- Whirl* – angular velocities in terms of local Krylov (Euler) angles [rad/s].

The dynamics of the ship under the action of external forces can be computed under the assumptions of the laws of rigid body motion. The algorithm therefore excludes consideration of hydroelasticity, sagging and hogging in waves, and other effects due to their assumed insignificance. Formally, this means that it is only necessary to calculate the total vector of forces and the point of its application. For the case of volumetric hydrostatic calculations, this is the volume within the wetted hull surface with the point of application of the buoyancy force at the instantaneous center of buoyancy. As a instantaneous force vector, it is directed along the normal to the averaged surface of the wave cut by the ship's hull:

$$\vec{B} = i\vec{V} \cdot \vec{v}\vec{W} \quad [m^3]$$

The vertical vector of gravity forces (weight) is defined in the global basis:

$$\vec{W} = \{0, 0, Volume\} \quad [m^3]$$

The translational velocity of the hull in the ship coordinate system and without attenuation due to the action of rotational torque because of misalignment between the external force and the ship's center of gravity:

$$\vec{V}+ = g \cdot \left( \vec{B} + \vec{W} / \vec{r} \right) \cdot \delta t / Volume \quad [m/s]$$

where  $g$  is gravitational acceleration; dividing by ship's basis  $\vec{r}$  means vector conversion from the fixed global coordinate system to the body-fixed coordinate system.

The moment arm of buoyancy forces in the ship's coordinate system:

$$\vec{R} = \vec{v}\vec{B} - \vec{Gravity} \quad [M]$$

The angular momentum of the forces during the time  $\delta t$  also in the ship's frame of reference:

$$\vec{M} = g \cdot (\vec{R} \times \vec{B}) \cdot \delta t \quad [m^5/s]$$

The updated angular velocity vector of the ship motion is also determined in the ship's frame of reference:

$$\vec{\Omega}+ = \vec{M} \cdot \delta t / inMass \quad [rad/s]$$

Fast calculation of volume integrals for hydrodynamic forces under the assumption of Froude-Krylov hypothesis does not take into account water pressure differences on the opposite sides, and therefore we can make corrections to take into account the diffraction of the waves

approaching the vessel:

$$\vec{v}\vec{S} = \sum \delta \vec{f}; \quad [N \cdot kg \cdot m/s^2]$$

$$\vec{v}\vec{R} = \sum \vec{r} \times \delta \vec{f} \quad [N \cdot m, kg \cdot m^2/s^2]$$

where  $\delta \vec{f}$  is the impulse of the calculated force on one triangle on the surface of the instantaneous waterplane in the fixed global coordinate system,  $\vec{v}\vec{S}$  is the longitudinal and lateral components of drift forces due to water level differences at the ship's side. The point of drift forces action  $\vec{v}\vec{F}$  (area center of the waterplane).  $\vec{v}\vec{R}$  is the free vector of added moments of trim and yaw.

Each element of the ship's surface  $\vec{ds}$  [ $m^2$ ] is washed by a local fluid flow with velocity  $\vec{v}$  [m/s], determined by the translational  $\vec{V}$  and angular  $\vec{W}$  components relative to the ship's center of mass,

$$\vec{v}_s = \vec{V} + \vec{W} \times (\vec{L} - \vec{G}) \quad [m/s]$$

where  $\vec{L}$  [m] is vector of coordinates of the center of each triangular element in ship's coordinate system. The computational model is based on the use of the velocity of displacement of the area elements of the ship's surface.

The relative velocity of the flow near the ship's surface is calculated by vector addition of the velocities of the wave flow and the intrinsic velocity of the surface element on the moving hull in the ship's reference frame:  $\vec{v} = \vec{V}_w - \vec{v}_s$  [m/s], where  $\vec{v}_s$  is the translational motion of the ship surface element;  $\vec{V}_w$  is the velocity of the wave flow translated into the ship's reference frame:  $\vec{V}_w = \vec{V}_w / \vec{r}$ .

The normal component of the total velocity vector is obtained by the double scalar product with the element's unit normal:

$$\vec{v}_n = (\vec{n} \cdot \vec{v}) \cdot \vec{n} \quad [m/s]$$

The flow velocity vector along the ship's surface is obtained by a similarly double vector product:

$$\vec{v}_s = [\vec{n} \times \vec{v}] \times \vec{n} = \vec{v} - \vec{v}_n. \quad [m/s]$$

Changing sign (order) in the last vector product, we can construct vector  $\vec{v}_{\perp}$  for mirror reflection of speed from the surface  $\vec{n}$ :

$$\vec{v}_{\perp} = (\vec{n} \cdot \vec{v}) \cdot \vec{n} + \vec{n} \times [\vec{n} \times \vec{v}] = \vec{v}_n - \vec{v}_s. \quad [m/s]$$

In this case, the normal and tangent components of the force impulse  $\delta \vec{f}$ , based on the calculation of wave diffraction by a small elementary area (triangle), can be written in the following form. The normal component of the impinging flow is deflected from the computational element of the surface, which is consistent with the zero normal-flow conditions. The value of the vector of the deflected external flow is applied as an inverse relationship with pressure by analogy with Torricelli's law, in which the hydraulic head (pressure) is elevated with the oncoming flow and calculated as a scalar product, and, accordingly, negative with reverse flow — as if with "fluid suction" from the ship's surface.

$$\frac{\delta \vec{f}_n}{\rho} = \frac{\Delta p_n}{\rho} \cdot \vec{ds} = \frac{(\vec{n} \cdot \vec{v}_n) \cdot |\vec{n} \cdot \vec{v}_n|}{2} \vec{ds} \quad [m^2/s^2]$$

where  $p$  is the pressure change on the surface element.

Bernoulli's formula for dynamic pressure is used for the tangent component. It is measured from a fixed pressure for the instantaneous velocity of the ship:

$$\frac{\delta \vec{f}_t}{\rho} = \frac{\Delta p_t}{\rho} \cdot \vec{ds} = \frac{V^2 - |\vec{n} \times \vec{v}_s|^2}{2} \vec{ds} \quad [m^2/s^2]$$

where  $V$  is the ship speed.

And in general:

$$\frac{\delta \dot{f}_\Delta}{\rho} = \frac{p_\Delta}{\rho} \cdot \delta \dot{s} = \left( \frac{V^2 - |\vec{n} \times \vec{v}_s|^2}{2} + \frac{\pm(\vec{n} \cdot \vec{v}_n)^2}{2} \right) \cdot \delta \dot{s} \quad [m^2/s^2]$$

In the latter expression, the dual products for  $\vec{v}_s$  and  $\vec{v}_n$  are simplified, since only velocity magnitudes are required to estimate the pressure changes in fluid flow, without regard for their spatial orientation.

Note that taking the ship's velocity  $\vec{V}$  as a reference, the shear component  $\vec{v}_s$  of the velocity will determine as a small hull sub-surface. If necessary, it can be compensated by including a slightly higher hull streamline velocity  $\vec{V}_\infty$  in the middle widest part of the hull (in the area of amidships). The normal velocity component  $\vec{v}_n$  always creates a negative trimming moment on the moving ship. It can be used to estimate conditions of planing over waves for specially shaped hulls.

The algorithm for calculations of velocity vectors and corrections to incident flow fluid pressures on the elementary triangles on the ship's surface form the basis for various simulations of impacts of oncoming and wave flows on the hull. Ship generated waves in the computational simulation are supplemented by storm wave diffraction forces together with simplified hydrodynamic action and reaction force effects on ship propulsion and motions.

The differential equations of small free oscillations of the ship include inertial and damping components for local restoring and drift forces and moments (Voitkunski, 1985). For example, the equations for rolling, pitching and heaving are:

$$\ddot{\theta} + 2\nu_\theta \dot{\theta} + \omega_\theta^2 \theta = 0, \quad [\text{rad}/s^2]$$

$$\ddot{\psi} + 2\nu_\psi \dot{\psi} + \omega_\psi^2 \psi = 0, \quad [\text{rad}/s^2]$$

$$\ddot{\zeta} + 2\nu_\zeta \dot{\zeta} + \omega_\zeta^2 \zeta = 0 \quad [m/s^2]$$

In extreme waves conditions, natural oscillations are neglected compared to the actions of steep irregular waves. Let us revise the equations for the other components:  $\chi$  – yawing;  $\eta$  – swaying;  $\xi$  – surging, resulting in canonical forms for these decaying oscillations:

$$\ddot{\chi} + 2\nu_\chi \dot{\chi} = 0, \quad [\text{rad}/s^2];$$

$$\ddot{\xi} + 2\nu_\xi \Delta \dot{\xi} = 0, \quad \ddot{\eta} + 2\nu_\eta \dot{\eta} = 0, \quad [m/s^2]$$

where:  $\dot{\xi}_i$  – is the forward speed based on indicated power of the engines in calm water,  $\Delta \dot{\xi} = \dot{\xi} - \dot{\xi}_i$  – oscillation of speed relative to propulsion in calm water.

In the discriminant of the canonical equations of motion there remains only a positive damping value  $\sqrt{\nu^2} = |\nu|$ . Thus, the fundamental solution in general reduces to damped oscillations of angular and translational velocities of the hull's motion, which in local coordinates is true for motions in all six degrees-of-freedom.

$$+\xi_+ = \dot{\xi}_i \delta t + \frac{\Delta \dot{\xi}}{2\nu_\xi} (1 - e^{-2\nu_\xi \delta t}) - \text{surge}, \quad [m]$$

$$+\eta_+ = \frac{\dot{\eta}}{2\nu_\eta} (1 - e^{-2\nu_\eta \delta t}) - \text{sway}, \quad [m]$$

$$+\zeta_+ = \frac{\dot{\zeta}}{2\nu_\zeta} (1 - e^{-2\nu_\zeta \delta t}) - \text{heaving}, \quad [m]$$

where  $\delta t$  is the calculated time interval of one step of the simulation,  $+\xi_+$ ,  $+\eta_+$  and  $+\zeta_+$  is the location of ship's center of mass at the end of the calculated time interval  $\delta t$ .

$$+\theta_+ = \frac{\dot{\theta}}{2\nu_\theta} (1 - e^{-2\nu_\theta \delta t}) - \text{changing of roll angle}, \quad [\text{rad}]$$

$$+\psi_+ = \frac{\dot{\psi}}{2\nu_\psi} (1 - e^{-2\nu_\psi \delta t}) - \text{increment of pitch}, \quad [\text{rad}]$$

$$+\chi_+ = \frac{\dot{\chi}}{2\nu_\chi} (1 - e^{-2\nu_\chi \delta t}) - \text{yaw, deviation from the course.} \quad [\text{rad}]$$

The damping factors can be interactively changed during the computational experiment. The initial conditions are initialized with numerical vectors as:

$$\nu_{\xi, \eta, \zeta} = \{ 0.05, 0.4, 0.3 \} - \text{for surge, sway, heave}$$

$$\nu_{\theta, \psi, \chi} = \{ 0.1, 0.3, 0.4 \} - \text{for roll, pitch, yaw}$$

The shape of the ship's hull above the water line may have large flat planes and an elevated superstructure. In cases of large roll angles and at the moments of capsizing, these surfaces concentrate hydrodynamic impact loads. To maintain the stability of the computational process, the roll rate is artificially limited so that the capsizing does not occur in less than 10 s. At the same time, the roll damping factor is quadrupled for the inverted hull position:

$$+\theta = 1 - (0.5625\theta/\pi)^2.$$

Krylov (Euler) angles are used in the construction of the computational process, which is characterized by the presence of a critical direction. It is conditioned in calculations by achieving the pitch for the ship. To avoid discontinuous geometric solutions, the pitch value is artificially limited to 84°.

An important function of the computational experiment is the smooth control of the rate of speed change, as well as limitation of the yaw rate when approaching a given heading, which does not limit the free dynamics of propulsion and yawing on the heading under the influence of storm waves.

Modeling these functions can be carried out based on separate models for propulsion, consistent with models for external actions (waves, wind), as part of a problem-oriented environment known as the virtual testbed. For a description of the components, see <http://shipdesign.ru>.

The ship's course is controlled by propeller thrust and smooth course control that makes it possible to simulate the occurrence of a heel with turning, running trim, acceleration and stopping. It also allows the simulation of speed loss in extreme seas, loss of heading control and broaching in following waves and other effects of motion and propulsion in all six degrees of free motion of the ship.

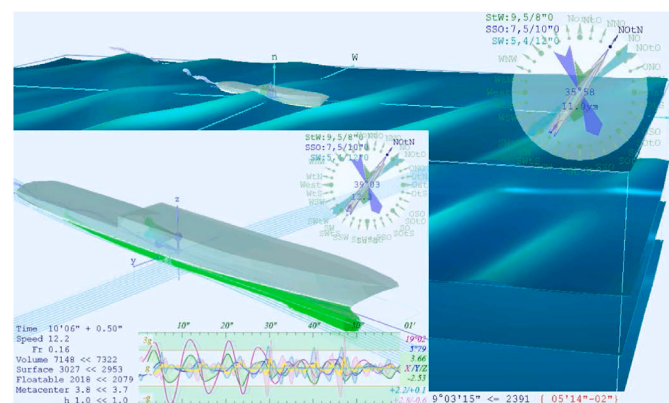


**Fig. 16.** During the computational experiment, two graphical windows are used to represent ocean waves and ship motions, as well as the ship hull with metacentric marks.

The linear damping in ship motion simulations is quite adequate for small speed deviations in waves relative to the ordered speed  $\dot{\xi}_i$  in calm water. It is possible to speed up the return to the ordered speed in case of large mismatches between the commanded and current speeds, without significant influence on its small surge oscillations. For this purpose, the algorithm provides a small increase in the damping factor.

$$+\xi_i / = (1 - \tanh^2(\dot{\xi}_i - \dot{\xi}) / 16) / 24.$$

Course (heading) control is performed by small increments of the heading  $\delta\chi$ , which in calm water provides full turn in one of three modes: "Rudder hard over" - in 1 min; "Rudder half over" - 2 min; and "Slower" - in 4 min. In rough seas, the "Slower" mode is activated automatically when the ship deviates from the set course by 1 rhomb ( $11^\circ 15'$ ), but this may not be sufficient to return the ship to the commanded heading. To speed up the turn and get the ship back on course, manual control can be used by selecting "Rudder hard over" or "Rudder half over" modes. After the ship has reached the specified course, the rudder is automatically set straight, with resumption of automatic control with rudder shifting to the "Slower" mode.

In the large graphical window (Fig. 16) it is possible to draw the entire wave field, the ship and the ship's path for visualization of the computational experiment. In the upper lines the current modes of sea wave and ship hydromechanics modeling are recorded. In the lower line the current computer time and the number of performed cycles. Red counts of minutes mean the lack of computational resources, and the lag of the computational experiment from the required real time.

The graphs on Fig. 16 show heave (green line with shading), roll (purple) and pitch (blue) values, as well as vertical accelerations at the center of gravity of the hull (yellow curve) and at its ends (blue curve with shading). You can control the heading of the modeled ship from any of the graphical windows. On the image with the ocean waves the group structure of the ocean waves and methods of their modeling are interactively constructed. In the window showing the ship the appropriate settings attitude (draft, heel, trim) stability, hull damping and selection of the hydromechanics models for the ship's exciting forces by the ocean waves are performed.

## 10. Results of computational experiments

The implementation of a highly efficient direct computational experiment for modeling the seakeeping hydromechanics of a ship using modern computer technology with advanced graphic capabilities makes it possible to visualize the seaworthiness of a ship in extreme seas. It is useful for ship's officers for identifying efficient and safe routes on the high seas and is especially necessary while optimizing the ship's lines and general ship arrangements for promising ships and vessels.

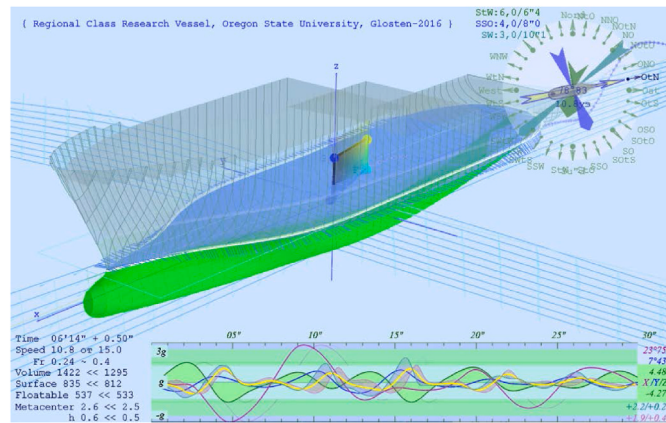


Fig. 17. Process of computational experiment in the window for a ship's hydromechanics representation.

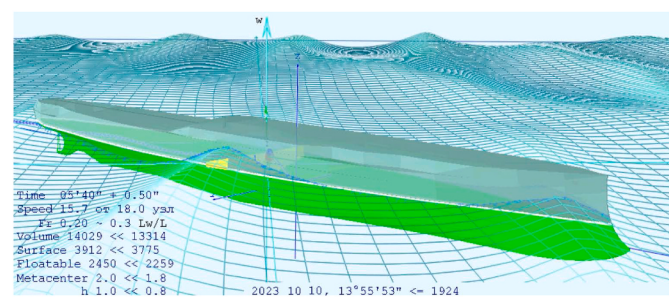


Fig. 18. "Ship 'Ryurik-2' in heavy trochoidal waves" – reproduction of ocean waves in a storm sea simulation. A contour drawing of the trochoidal wave profiles with steep slope are superposed on a long-period swell of comparable height.

Let us give some examples of the implementation of the proposed approach in the form of a problem-oriented environment, a "virtual testbed". It consists of a combination of highly efficient computational algorithms, a database of ship hulls, statistical characteristics of wind fields for different seasons and regions of the World Ocean, and a graphical interface for interactive work.

The translucent hull (Fig. 17) reveals the surface of the waterplane. Large circles mark the active center of the waterplane area - blue; center of buoyancy - blue; center of gravity - dark blue; and the metacenter green when the metacentric height increases, yellow when it decreases, and red when it is negative. Small circles mark the initial values in still water, arrows from them point to the large circles marking the instantaneous locations of the metacenters. On the compass rose at the top right, one can see the rudder angle, with hard-over to the right. This reflects the command from the autopilot in response to strong yaw. Navigation parameters are given at the bottom left: current time and calculated step; a commanded calm water speed of 15 knots; an achieved speed in large waves of 10.8 knots; and other inertial and metacentric characteristics. Along the trajectory of the ship's origin, heave and surge at the instant of extreme roll are visible.

In the bottom portion of the graphic window is a plot of roll, pitch and heave over a sliding time interval, with the time axis in seconds. The right scale shows extrema for roll and pitch on a single scale, red - roll (X), blue - pitch (Y). For heave measured from the center of buoyancy, the extrema are reduced to half the vertical scale of the graph. The heave (Z) is plotted in green.

The thick yellow curve shows the vertical accelerations at amidships, flanked by shading showing the accelerations at the ends. The fixed acceleration scale is shown on the left side of the graph it ranges from  $-1g$  to  $+3g$ . This acceleration includes the vessel's weight, so if the acceleration is zero, loose cargo would be weightless and leave the deck.

An important element of the methodology for building a series of computational experiments is the ability to specify initial conditions based on certain geometric or hydrodynamic criteria. For this purpose, in addition to interactive control of the ship's heavy weather performance, it is possible to use special initializing text files, in which initial conditions and the selection keys for mathematical models can be specified both as absolute spatial or temporal values and as measurements relative to wave or ship dimensions. The single initialization file for all models is called Vessel.vil (vessel-initiation + logging), and the same as the Model-Name.vil file — for a particular ship model. During the computational experiment, the configuration file is supplemented by a protocol with the results of simulation of the seaworthiness and controlled maneuvering of the ship in ocean wave conditions.

## 11. Conclusion

Direct computational experiments for a ship navigating in extreme seas, with the ability to visualize the hydromechanics of interaction with realistic, severe seas in real time, can serve as a justification for the

design of ships and vessels with increased seaworthiness in heavy seas. These tools are also useful as part of an on-board navigational computer or expert information system in maritime service as crew-mentors, for the synthesis of operational recommendations to mariners in difficult and stormy conditions.

The experimental computing environment includes a full-fledged three-dimensional visualization of the structure of ocean waves, with the trajectory and instantaneous position of a ship, along with visualization of the instantaneous hydrodynamic centers and metacentric parameters showing the variation of stability.

Standard OpenGL graphical tools make it possible to adjust the transparency of ocean waves with a choice of options of solid or contour drawings of the ship's lines and the ship's surface architecture. This gives the ship's officers the opportunity to visually analyze and predict in advance the conditions and effectiveness of a given course through a storm, including the prevention of potentially dangerous or emergency situations in high seas.

The new toolkit opens a novel direction of research in the field of ship hydromechanics. Significant advantages of such a "virtual testbed" are specification of the optimal amount of computer memory and computing performance, which makes it possible to recommend new software systems for wide use in design studies and production; for research and academic purposes.

## CRediT authorship contribution statement

**Alexander Degtyarev:** Conceptualization, Formal analysis, Investigation, Methodology, Writing – original draft, Writing – review & editing. **Vasily Khramushin:** Conceptualization, Investigation, Methodology, Software, Validation, Visualization.

## Declaration of competing interest

The authors declare that they have no known competing financial interests or personal relationships that could have appeared to influence the work reported in this paper.

## Data availability

Data will be made available on request.

## Acknowledgement

The work described in this paper has partially been supported by Saint-Petersburg State University (research project 95438429) and by US Office of Naval Research Global in 2015 under its visiting scientist program under supervision of Dr. Woei-Min Lin. The authors are grateful to Dr. Art Reed and Mr. Kenneth Weems of David Taylor Model Basin for fruitful discussions and help with the paper.

## Appendix

Let us introduce geometrical notations adopted in this work ([Khramushin, 2005](#)).

Local tensor in the absolute frame of reference is written as a string of three basis vectors or three-column coordinate matrix (index at a vector on the right):

$$\hat{\vec{r}} = \vec{r}_i = \left\{ \vec{r}_1 \quad \vec{r}_2 \quad \vec{r}_3 \right\} = \begin{Bmatrix} r_{1,1} & r_{1,2} & r_{1,3} \\ r_{2,1} & r_{2,2} & r_{2,3} \\ r_{3,1} & r_{3,2} & r_{3,3} \end{Bmatrix}$$

Projections of simple basis vectors of global coordinate system in local basis are represented uniquely in the form of dual basis  $\overset{\vee}{\vec{r}} = \overset{\leftarrow}{\vec{r}}^j = \hat{\vec{r}}^{-1}$  (or inverse matrix)

$$\overset{\vee}{\vec{r}} = \overset{\leftarrow}{\vec{r}}^j = \begin{Bmatrix} \overset{\leftarrow}{\vec{r}}^1 \\ \overset{\leftarrow}{\vec{r}}^2 \\ \overset{\leftarrow}{\vec{r}}^3 \end{Bmatrix} = \begin{Bmatrix} r^{1,1} & r^{2,1} & r^{3,1} \\ r^{1,2} & r^{2,2} & r^{3,2} \\ r^{1,3} & r^{2,3} & r^{3,3} \end{Bmatrix} = \hat{\vec{r}}^{-1}$$

$\vec{A} = \vec{R} + \vec{a} = \mathbf{A}_i$  vector with covariant components where the capital letter  $A$  means that a vector is constructed, measured relative to a common center  $\Omega$  and scaled in a uniform global coordinate system. If arrow is to the right  $\rightarrow$  or the vector index is at the bottom (subscript), then vector components are projected onto the coordinate axes of the global reference system. If an arrow is to the left or vector index is at the top (superscript)  $\overset{\leftarrow}{\vec{A}} = {}_{\Omega}\mathbf{A}^j$  then the vector components are contravariant. They are projected in the dual system of local coordinates  $\overset{\vee}{\vec{r}}$  inside a large fluid particle. The one-to-one association between dual basis is defined by a multiplication operation with a tensor in the form of a concrete fundamental particle:  $\vec{R} = \hat{\vec{r}} \cdot {}_{\Omega}\vec{R}$  or  ${}_{\Omega}\vec{R} = \vec{R}/\hat{\vec{r}} = \vec{R} \bullet \hat{\vec{r}}$ .

The left-hand indexes unless otherwise stated can be used for space binding of computing objects and to mark it in current time:

${}_{\Omega}\vec{R}$  are coordinates of knot point.  $\Omega$  defines location of node in mesh of computational domain;  $T$  is time from the beginning of the computational experiment.

${}_{+}^t\vec{R}$  is reference to adjacent point (relative to the direction '+' starting from the center of mass of the large fluid particle  $\Omega$  offset in time by an amount  $t$ ).

$\vec{A} = A_i$  – space point (vector) marked in global coordinate system [m];

$\vec{a} = a^k$  – vector counting in the local basis of an elementary fluid particle [ $m^{-2}$ ];

$\hat{\vec{r}} = \vec{r}_k = r_{ik}$  – tensor of form of large fluid particle [ $m^3$ ];

$\overset{\vee}{\rho} = \overset{\leftarrow}{\rho}^j = \rho^{kj}$  – tensor of density [ $kg \cdot m^{-3}$ ];

$\overset{\leftarrow}{M} = M_j^i = \overset{\vee}{\rho} \cdot \overset{\wedge}{r}$  – mixed tensor which relates the internal state of the particle in the global reference system [kg];

In this case it is possible to present a brief table of general notations.

$T$ – absolute time counting; $t = \Delta T$ – calculated time interval	c
$p$ – pointwise (scalar) pressure,	N/m <sup>2</sup>
$\underline{\Omega} \vec{R}$ – coordinates of knot of mesh area $\Omega$ at time instant T	m
$\underline{+} \vec{R}$ – coordinates of adjacent point at the next time instant	m
$\vec{V}$ – velocity of fluid particle in global reference system	m/s
$\bar{v}$ – velocity in global basis for a fluid particle with local scale	m/s
$\vec{w}$ – vector of velocity increment ( <i>acceleration</i> ) for fluid particles	m/s <sup>2</sup>
$\hat{r} = \vec{r}_i = r_g$ – geometric tensor for the form of a large fluid particle	m <sup>3</sup>
$\hat{v} \cdot t = \vec{v}_i \cdot t = \underline{+} \vec{r}_i = \underline{+} \vec{r}_i - \underline{\Omega} \vec{r}_i$ – tensor of local velocities ( <i>coordinate increments</i> ), as the deformation of the basic axes of the geometric tensor	m <sup>3</sup>
$\hat{v} = \underline{+} \vec{v}$ – tensor of convective velocities	1/s
$\hat{w} = \underline{+} \vec{v}_i$ – tensor of flow inside large fluid particle	m <sup>3</sup> /s
$\hat{\rho} = \bar{\rho}^v = \rho^{kj}$ – tensor of density or internal state of fluid particle	kg/m <sup>3</sup>
$\hat{m} = m_j^i = \hat{\rho} \cdot \hat{r}$ – tensor mass of fluid particle (mixed tensor resulting internal state of fluid to global frame of reference)	kg
$\vec{F}$ – resultant vector of mass (volume) forces	N
$\vec{f} = \vec{w} \cdot \hat{m} = \vec{w} \cdot \hat{\rho} \cdot \hat{r}$ – to the law of motion for a free particle in a continuous medium	N
$\hat{f}$ – tensor of stresses at the boundaries of fluid particle	N·m <sup>2</sup>
$\hat{s} = \hat{f} \cdot \hat{r}$ – stress inside and in a vicinity of fluid particle	N/m
$\hat{s}_H = \hat{v}_H \cdot \hat{\eta} / \lambda$ – Newton's conditional viscous stress tensor	N/m
$\eta$ – dynamic viscosity tensor	N·s/m <sup>3</sup>
$\tau = \eta \cdot \hat{p}$ – tensor of kinematic viscosity coefficients	m/s
$\hat{s}_T = \hat{v}_T \cdot \hat{\kappa} / \lambda$ – elastic stress tensor according to Hooke's linear law:	N/m
$\kappa$ – dimensional tensor of elasticity (stiffness)	N/m <sup>3</sup>
$\mu = \kappa \cdot \hat{p}$ – tensor modulus of volumetric and shear elasticity	m
$\mu$ – dimensionless Poisson's modulus for mutually normal strains	

## References

- Abrashkin, A.A., Pelinovsky, E.N., 2022. Gerstner waves and their generalizations in hydrodynamics and geophysics. *Phys. Usp.* 65, 453–467. <https://doi.org/10.3367/UFNe.2021.05.038980>.
- Methods in computational physics: advances in research and applications. In: Alder, B., Fernbach, S., Rotenberg, M. (Eds.), 1964. *Fundamental Methods in Hydrodynamics*, 3. Academic Press.
- Anastopoulos, P.A., Spyrou, K.J., Bassler, C.C., Belenky, V., 2015. Towards an improved critical wave groups method for the probabilistic assessment of large ship motions in irregular sea. *Probabilist. Eng. Mech.* 44, 18–27.
- Balashov, V.A., Borisov, V.E., Khankhasaeva, Ya.V., 2018. An implicit scheme based on the LU-SGS method for URANS equations with SST turbulence model. *Preprints of Keldysh Institute of Applied Mathematics* 31, 20. <https://doi.org/10.20948/preprint-2018-31>.
- Belocerkovskiy, O.M., Davidov, Yu.M., 1982. *Method Of Large Particles in Gas Dynamics*. M. Nauka (in Russian).
- Boccotti, P., 2000. *Wave Mechanics for Ocean Engineering*. Elsevier Science, Oxford, p. 496, 9780080543727.
- Boccotti, P., 2014. *Wave Mechanics and Wave Loads on Marine Structures*. Butterworth-Heinemann, Elsevier, p. 344.
- Bogdanov, A., Degtyarev, A., Gankevich, I., Khrushin, V., Korkhov, V., 2020. Virtual testbed: concept and applications. *Lect. Notes Comput. Sci.* 12254, 3–17. [https://doi.org/10.1007/978-3-030-58817-5\\_1](https://doi.org/10.1007/978-3-030-58817-5_1). Springer.
- Boukhannovsky, A., Rozhkov, V., Degtyarev, A., 2001. Peculiarities of computer simulation and statistical representation of time-spatial metocean fields. *Lecture Notes in Computer Science*, Springer 2073, 463–472. [https://doi.org/10.1007/3-540-45545-0\\_55](https://doi.org/10.1007/3-540-45545-0_55).
- Box, G.E.P., Jenkins, G.M., Reinsel, G.C., 2008. *Time Series Analysis: Forecasting and Control*, fourth ed. Wiley, p. xx+746.
- Degtyarev, A., Boukhannovsky, A., 2000. Peculiarities of motion of ship with low buoyancy on asymmetrical random waves. In: Proc. Int'l. Conf. Stability of Ships and Floating Vessels, Launceston, Tasmania, Australia, 2, pp. 665–679.
- Degtyarev, A., Gankevich, I., 2011. Efficiency comparison of wave surface generation using OpenCL, OpenMP and MPI. In: Proc. 8th Int'l. Conf. Computer Science & Information Tech., Yerevan, Armenia, pp. 248–251.
- Degtyarev, A., Gankevich, I., 2015. Computation of pressures in inverse problem in hydrodynamics of potential flow. In: Proc. 12th Int'l. Conf. On Stability of Ships and Ocean Vehicles, Glasgow, pp. 1117–1122.
- Degtyarev, A.B., Gankevich, I., 2019. Evaluation of hydrodynamic pressures for autoregressive model of irregular waves. In: Belenky, V., Spyrou, K., van Walree, F., Neves, M.A.S., Umeda, N. (Eds.), Chapter 3 of *Contemporary Ideas on Ship Stability. Risk of Capsizing*. Springer, pp. 37–47, 978-3-030-00514-6.
- Degtyarev, A.B., Khrushin, V.N., 2014. Design and construction of computer experiment in hydrodynamics using explicit numerical schemes and tensor mathematics algorithms. *Math. Model.* 26 (11), 4–17.
- Degtyarev, A.B., Reed, A.M., 2013. Synoptic and short-term modeling of ocean waves. *Int. Shipbuild. Prog.* 60 (1–4), 523–553. <https://doi.org/10.3233/ISP-130091>.
- Degtyarev, A., Khrushin, V., Mareev, V., 2014. Design and construction of computer experiments in fluid mechanics and ship stability. *Proc., 14th International Ship Stability Workshop*, Kuala Lumpur, Malaysia, pp. 187–198.
- Degtyarev, A.B., Reed, A.M., Gankevich, I., 2019. Modeling of incident waves near the ship's hull (application of autoregressive approach in problems of simulation of rough seas). In: Belenky, V., Spyrou, K., van Walree, F., Neves, M.A.S., Umeda, N. (Eds.), Chapter 2 of *Contemporary Ideas on Ship Stability. Risk of Capsizing*. Springer, pp. 25–35, 978-3-030-00514-6.
- Degtyarev, A., Gankevich, I., Kulabukhova, N., Khrushin, V., 2020. Computational model of unsteady hydromechanics of large amplitude Gerstner waves. *EPJ Web Conf.* 226 (1–4), 02009 <https://doi.org/10.1051/epjconf/202022602009>.
- Frank, W., 1967. Oscillation of cylinders in or below the free surface of deep fluid. *Naval Ship Research and Development Center. Rep* 2375, 42.
- Gerstner, F., 1809. Theorie der wellen. *Ann. Phys.* 32, 412–445.
- Gong, Jiaye, Li, Yunbo, Dai, Kun, Fu, Zheng, Hong, Zhichao, 2022. Numerical simulation of ship maneuvering by a hybrid method with propulsive factors in waves taken into account. *Ocean Eng.* 264, 112538.
- Gurgenidze, A.T., Trapeznikov, Y.A., 1988. Probabilistic model of wind waves. In: *Theoretical Foundations and Methods of Calculating Wind Waves*. Leningrad. Gidromet-eoizdat, pp. 8–23 (in Russian).
- Khaskind, M.D., 1973. *Hydrodynamic Theory of Ship Motion*. Nauka, Moscow, p. 328 (in Russian).
- Khrushin, V.N., 2005. *3D Tensor Mathematics for the Computational Fluid Mechanics Experience*. Vladivostok: FEB RAS, (in Russian).
- Kochin, N.E. (Ed.), 1965. *Vector Calculus and Beginnings of Tensor Calculus*, 9th M. Nauka (in Russian).
- Krylov, A.N., 1951. *Collected Works*, V. 11 *Ship Motion*. Pub. USSR Academy of Sciences, p. 183.
- Lamb, H., 1975. *Hydrodynamics*, sixth ed. Cambridge Univ.Pres.
- Longuet-Higgins, M.S., 1962. The statistical analysis of a random, moving surface. *Phil. Trans. Roy. Soc. Lond. Math. Phys. Sci.* 249 (966), 321–387.
- Lugovski, V.V., 1980. *Hydrodynamics of Nonlinear Ship Motion*. Sudostroenie, Leningrad, p. 256 (in Russian).
- Lugovski, V.V., 1995. Mathematical models for discovering of nonlinear ship motion stability on waves. In: Proc. Int. Symp. On Ship Hydrodynamics, St. Petersburg, pp. 83–91 (in Russian).

- Newman, J.N., 1970. Application of Slender-body theory in ship hydrodynamics. *Annu. Rev. Fluid Mech.* 2, 67–94.
- Ortega, J.M., 2013. *Introduction to Parallel and Vector Solution of Linear Systems*. Springer, New York, NY.
- Patankar, S.V., 1991. *Computation of Conduction and Duct Flow Heat Transfer*. Innovative Research Inc.
- Pipiras, V., Reed, A., Sapsis, T., Weems, K., 2023. Longuet-Higgins wave model and ARMA representations. *Proc., of the 19<sup>th</sup> Intl. Ship Stability Workshop*, pp. 141–148.
- Pletcher, R.H., Tannehill, J.C., Anderson, D.A., 2013. *Computational Fluid Mechanics and Heat Transfer*, third ed. CRC Press, Taylor & Francis Group.
- Rosenblatt, M.A., 1957. Random model of the sea surface generated by the hurricane. *J. Math.* 6, 235–246.
- Rozhkov, V.A., Lyashenko, A.F. (Eds.), 1990. *The Results of Oceanological Research in Tropical East Pacific*. Hydrometeoizdat, Leningrad, p. 293 (in Russian).
- Rozhkov, V.A., Trapeznikov, Y.A., 1990. *Probabilistic Models of Oceanographic Processes*. Gidrometeoizdat, Leningrad (in Russian).
- Shin, Y.S., Belenky, V.L., Lin, W.M., Weems, K.M., Engle, A.H., 2003. Nonlinear time domain simulation technology for seakeeping and wave-load analysis for modern ship design. *SNAME Trans.* 111, 557–578.
- St. Denis, M., Pierson, W.J., 1953. On the motion of ships in confused seas. *Trans. SNAME* 61, 280–354.
- Sveshnikov, A.A., 1959. Determination of the probability characteristics of three dimensional sea waves. *Math. Akad. Mech. Eng.* 3, 32–41.
- Ship theory handbook. In: Voitkunski, Y.I. (Ed.), 1985. *Statics of Ship, Ship Motion*, 3 Volumes vol. 2. Sudostroenie, Leningrad, p. 440 (in Russian).
- Weems, K., Reed, A.M., Degtyarev, A.B., Gankevich, I., 2016. Implementation of an autoregressive wave model in a numerical simulation code. *Proc., 31st Sym. Naval Hydro*. Monterey, California, USA, p. 12.
- Yu, Jiawei, Yao, Chaobang, Huang, Jianghao, Dong, Guohua, Zhang, Zhiguo, Feng, Dakui, 2023. Assessment of different hybrid methods for simulations of free running surface ship maneuvering in waves. *Appl. Ocean Res.* 139, 103703.
- Zommerfel'd, A., 1954. *Mechanics of Deformable Media*. M.: Foreign Literature Publishing House (in Russian).